

Stable water isotope simulation by current land-surface schemes: Results of iPILPS Phase 1

A. Henderson-Sellers^a, M. Fischer^{a,*}, I. Aleinov^b, K. McGuffie^c, W.J. Riley^d,
G.A. Schmidt^b, K. Sturm^a, K. Yoshimura^e, P. Irannejad^{a,f}

^a Institute for Nuclear Geophysics, Australian Nuclear Science and Technology Organisation, Lucas Heights Science and Technology Centre,
Private Mail Bag 1, Menai, NSW 2234, Australia

^b NASA Goddard Institute for Space Sciences and Columbia University, New York, NY 10025, United States

^c University of Technology, Sydney, Department of Applied Physics, Sydney, 2007, Australia

^d LBNL, Earth Sciences Division, Berkeley, CA 97420, United States

^e University of Tokyo, Tokyo, 153-8505, Japan

^f University of Tehran, Institute of Geophysics, 6466-14155, Iran

Received 18 June 2005; received in revised form 20 December 2005

Available online 20 March 2006

Abstract

Phase 1 of isotopes in the Project for Intercomparison of Land-surface Parameterization Schemes (iPILPS) compares the simulation of two stable water isotopologues ($^1\text{H}_2^{18}\text{O}$ and $^1\text{H}^2\text{H}^{16}\text{O}$) at the land–atmosphere interface. The simulations are offline, with forcing from an isotopically enabled regional model for three locations selected to offer contrasting climates and ecotypes: an evergreen tropical forest, a sclerophyll eucalypt forest and a mixed deciduous wood. Here, we report on the experimental framework, the quality control undertaken on the simulation results and the method of intercomparisons employed. The small number of available isotopically enabled land-surface schemes (ILSSs) limits the drawing of strong conclusions, but, despite this, there is shown to be benefit in undertaking this type of isotopic intercomparison. Although validation of isotopic simulations at the land surface must await more and much more complete, observational campaigns, we find that the empirically based Craig-Gordon parameterization (of isotopic fractionation during evaporation) gives adequately realistic isotopic simulations when incorporated in a wide range of land-surface codes. By introducing two new tools for understanding isotopic variability from the land surface, the isotope transfer function and the iPILPS plot, we show that different hydrological parameterizations cause very different isotopic responses. We show that ILSS-simulated isotopic equilibrium is independent of the total water and energy budget (with respect to both equilibration time and state), but interestingly the partitioning of available energy and water is a function of the models' complexity.

© 2006 Elsevier B.V. All rights reserved.

Keywords: water isotopes; land parameterization; model intercomparison; Craig-Gordon scheme; PILPS

1. iPILPS introduction

1.1. Background and timing

The goals of iPILPS are to (1) offer a framework for intercomparison of isotope-enabled land-surface

* Corresponding author.

E-mail address: ipilps@ansto.gov.au (M. Fischer).

schemes (ILSSs) and (2) encourage improvement of these schemes by evaluation against high-quality (isotope) observations. When iPILPS was approved by the GEWEX Land–Atmosphere System Study (GLASS) in September 2004 (Henderson-Sellers, 2006), it was agreed that its first stage (Phase 1) would focus on the stable water isotopes H_2^{18}O and $^1\text{H}^2\text{H}^{16}\text{O}$.

Phase 1 of this international project tests the hypothesis that: observation and analysis of the diurnal fluxes of $^1\text{H}_2^{18}\text{O}$ and $^1\text{H}^2\text{H}^{16}\text{O}$ between the soil, plants and atmosphere can accurately determine the partitioning of precipitation into transpiration, evaporation and total runoff (surface plus soil drainage). Although this hypothesis is not fully tested in this paper, the direction such testing could take is described in Henderson-Sellers (2006). The iPILPS effort will contribute (1) to improving the accuracy with which land-surface schemes partition net available surface energy into latent and sensible heat fluxes and thus (2) to decreasing uncertainty in hydroclimate modelling and water resource vulnerability predictions. Phase 1 of iPILPS exploits novel stable water isotopes (SWI) and analysis techniques in the development and evaluation of ILSSs. To achieve the project aims, it is necessary to:

- (1) identify and test ILSSs which already (or plan soon to) incorporate SWIs;
- (2) appraise SWI data applicable to hydroclimatic and water resource aspects of ILSSs;
- (3) identify observational data gaps required for evaluating ILSSs and resolve them; and
- (4) apply SWI data to specific predictions of well-understood locations simulated by available ILSSs.

The timeline for Phase 1 of iPILPS began in late 2004 with the distribution of the Phase 1 plan and call for participants (see Henderson-Sellers, 2006). The simulations were conducted over the period February to April 2005. The inaugural iPILPS Workshop from 18 to 22 April 2005 was held in Sydney and focussed on the first intercomparison results. Throughout Phase 1 of iPILPS, an interactive website is being used to manage the ILSS simulations from participants (<http://ipilps.ansto.gov.au>). This allows quick-look intercomparisons by the ILSS owners and rapid community-wide dissemination of results.

1.2. Forcing meteorology and isotopes

Offline simulations need appropriate boundary conditions. The ILSSs require either measured forcing

meteorology and isotopes or the same variables derived from a model representing atmospheric and isotopic processes as closely as possible to actual meteorological conditions. The meteorological and isotopic variables need to be coherent; deriving one from observations and the other from a model is not adequate.

For iPILPS Phase 1, it was determined that the only way of supplying adequately good forcing was to use an isotope-enabled atmospheric model. The REMO (REgionales MOdel, developed by the Max Planck Institute for Meteorology, Hamburg) had been shown to generate high-quality simulations for two of the three selected locations (Sturm et al., 2005, submitted for publication). The spatial resolution of REMO is 1/2 degree (~ 54 km) with a model timestep of 5 min. REMO is nested into the European Centre Hamburg GCM (ECHAM) and the iPILPS Phase 1 forcings were derived from nesting into the ‘climatological’ version of ECHAM, which had a constant annual cycle in sea-surface temperatures—see Fischer and Sturm (2006-this issue) for further details.

Even though weather systems are better represented in REMOiso than in a global model, running in a climatological mode does not permit reproduction of specific meteorological situations. Global reanalyses, which assimilate all available meteorological observations, are believed to provide the best estimation of the actual state of the atmosphere (e.g. Kistler et al., 2001), but no isotopic information is yet available in any reanalysis.

The simulations of REMOiso have been thoroughly analysed in its first domain, which covers the European continent, encompassing temperate, Mediterranean and subpolar climates (Sturm et al., 2005). Following this success, REMOiso was moved to the South American continent, including the Amazon, the arid grassland regions such as Brazil’s Nordeste and the Andes glaciers (Sturm et al., 2006-this issue). Most recently, REMOiso has been integrated over Australia spanning tropical monsoons in the north, the arid centre and to Mediterranean climates in the south (Fischer and Sturm, 2006-this issue). All these model evaluations have been successful for simulated precipitation and humidities and their isotopic signature and REMOiso parameterizations have been proved to be elaborate enough to adequately represent secondary effects such as the deuterium excess. Based on these experiments, we are confident that REMOiso performs well in all climatic environments selected for iPILPS.

The forcing data include magnitudes of each isotope (i.e. $^1\text{H}_2^{18}\text{O}$ and $^1\text{H}^2\text{H}^{16}\text{O}$) in precipitation and in water vapour at the atmospheric lowest level

plus all the standard (ALMA—Assistance for Land-surface Modelling Activities) meteorological forcing including ‘regular’ water ($^1\text{H}_2^{16}\text{O}$). Full details of the generation of these forcing data are given in Fischer and Sturm (2006—this issue) who also offer demonstrations that the simulations of REMOiso are of high quality.

1.3. Participating ILSSs

By the date of the first Phase 1 Workshop (April, 2005), five ILSSs had submitted simulations to the iPILPS web. Three other ILSSs were represented at the Workshop even though their simulations were not yet available. In this paper, results from the first five ILSSs only are compared, although the methodology used and recommended for future intercomparisons was derived with a broader ILSS community in mind. The five ILSSs whose simulations are included here are:

- (1) The REMOiso ILSS (Sturm et al., 2005)
- (2) The GISS ILSS (Aleinov and Schmidt, 2006)
- (3) Iso-MATSIRO (Yoshimura, 2006)
- (4) ICHASM (Fischer, 2006)
- (5) ISOLSM (Riley et al., 2002).

In all the intercomparisons presented here, these ILSSs are designated by a consistent letter (A–E). Note that the same letter always refers to the same model, but we do not reveal which of the models is letter “A”, for example. This anonymity is intentionally used to focus analysis on the strengths and weaknesses of the whole group of simulations rather than specific models. Naturally, all ILSS owners are aware of their model’s performance and some aspects of these are described in detail in the papers in this volume listed above.

2. Experimental plan for Phase 1

2.1. Outline

It was planned to undertake iPILPS ILSS’ evaluation in two stages, each with two parts:

- (1) spin-up and conservation check simulations:
 - (a) gross water and energy
 - (b) stable water isotopologues (SWIs): $^1\text{H}_2^{18}\text{O}$, $^1\text{H}^2\text{H}^{16}\text{O}$ and $^1\text{H}_2^{16}\text{O}$; and
- (2) comparison and evaluation with observations:
 - (a) monthly means and annual cycles
 - (b) diurnally resolved simulations.

Although the main aim of iPILPS Phase 1 is ILSS simulations’ intercomparison, sites for simulation have been selected which cover a range of climatologies, and for which there are high-resolution meteorological and some isotopic observations available. Unfortunately, it has proved impossible to identify diurnal isotopic observations of high enough quality to add value, although this study has prompted a recent Australian campaign in Tumberumba (Twining et al., 2006).

The three selected locations for iPILPS Phase 1 are:

- (1) mid-latitude (deciduous) grass/woods, nominally at Munich 48°N 11°E
- (2) tropical (evergreen) rainforest, nominally at Manaus 3°S 60°W
- (3) mid-latitude eucalypt (evergreen) forest, nominally at Tumberumba 35°S 148°E.

A general description of the geo-ecology and climatology of each location is provided on the iPILPS website (<http://ipilps.ansto.gov.au>). Forcing was provided for the three locations for four years. The experimental design directed each ILSS to use the first year’s forcing repeatedly for as many years as that ILSS required to achieve equilibrium (this experimental component was designated EQY1), and then use the next three years’ forcing to create three years’ simulations (this ‘Basin Comparison’ was designated BC24).

2.1.1. Equilibration experiment (EQY1)

Each ILSS initialized water reservoirs at half capacity (except snow capacity, which is infinite in all participating schemes and hence initialized with zero H_2O), all water isotope reservoirs at VSMOW and all temperatures at the supplied annual mean surface air temperature. Then the REMOiso Year 1 forcing was applied over as many repeated years as required to reach equilibrium. Equilibrium was defined as in PILPS 2a (Cabauw—see Chen et al., 1997). That is, for bulk water and energy, equilibrium was defined as being the first occasion on which the January mean values of surface radiative temperature, latent and sensible heat fluxes, and root zone soil moisture did not change by more than 0.01 K, 0.1 W m^{-2} and 0.1 kg m^{-2} , respectively, from year N to year $N+1$. The equilibration time was then N years.

In this first iPILPS experiment, no criteria were specified for isotopic equilibrium, but some model owners applied their own criteria (that is, that the isotopologue mass changes were less than a sufficiently small, but generally arbitrary, value). The main goal of

EQY1 was setup and equilibration to ensure gross water and energy conservation but the design allowed a secondary goal: the determination of spin-up times and trajectories for SWIs, once the gross water mean state was confirmed as equilibrated.

2.1.2. Grid-point/site scale comparison (and ultimately evaluation) (BC24)

For each ILSS, the REMOiso years 2 to 4 were applied sequentially starting from the conditions achieved after EQY1. For this experimental component, the planned goal was site-specific diurnal comparison and also evaluation against available observational data. Following exhaustive searches, it has been determined that no diurnal observations of adequate quality exist for these locations. At this time, the analysis is therefore limited to ILSS intercomparison. However, it is hoped to undertake monthly mean basin-scale comparison and evaluation against observations from Global Network for Isotopes in Precipitation (GNIP) and the Global Network for Isotopes in Rivers (GNIR) programmes.

2.2. Data protocols

2.2.1. ALMA (Assistance for Land-surface Modelling Activities)

As part of GLASS's PILPS, iPILPS uses the ALMA convention for variable names, units and signs (http://www.lmd.jussieu.fr/~polcher/ALMA/convention_3.html). We opted to use ALMA's 'traditional' format for model output (http://www.lmd.jussieu.fr/~polcher/ALMA/convention_output_3.html).

As many variables, especially the isotopic ratios, did not have existing ALMA conventions, we extended the ALMA conventions to include new variable names. Some of these new variable names are based on the NCEP/NCAR reanalysis data conventions: <http://www.cdc.noaa.gov/cdc/data.ncep.reanalysis.html>. The new variables are listed in Tables 1 and 2.

2.3. Model forcing and model output

The model forcing described here includes both atmospheric forcing and time-invariant surface properties. The time-invariant surface properties likely to be needed for each location simulated, such as vegetation type specifications and soil property specifications, were provided and are listed in Table 3.

The forcing variables for iPILPS Phase 2 experiments provided by the Regional Isotope Model (REMOiso) are listed in Table 1. The forcing data has

Table 1
Variables provided from REMOiso as forcing for the ILSSs

Model forcing	ALMA		
	Name	Units	+Sign ^a
Large-scale precipitation rate (H ₂ ¹⁶ O)	PRECL16 ^b	kg m ⁻² s ⁻¹	Downward
Convective precipitation rate (H ₂ ¹⁶ O)	PRECC16 ^b	kg m ⁻² s ⁻¹	Downward
Atm bottom level ^c temperature	Tair	K	N/A
Downward short-wave rad onto surface	Swdown	W m ⁻²	Downward
Downward long-wave rad onto surface	Lwdown	W m ⁻²	Downward
Atm bottom level specific humidity (H ₂ ¹⁶ O)	Qair	kg kg ⁻¹	N/A
Atm bottom level zonal wind	Wind_E	m s ⁻¹	Eastward
Atm bottom level meridional wind	Wind_N	m s ⁻¹	Northward
Atm surface pressure	Psurf	Pa	N/A
Energy of precipitation	Qrain	W m ⁻²	Downward
Large-scale precipitation H ₂ ¹⁸ O	PRECL18 ^b	kg m ⁻² s ⁻¹	Downward
Large-scale precipitation HDO	PRECLD ^b	kg m ⁻² s ⁻¹	Downward
Convective precipitation H ₂ ¹⁸ O	PRECC18 ^b	kg m ⁻² s ⁻¹	Downward
Convective precipitation HDO	PRECCD ^b	kg m ⁻² s ⁻¹	Downward
Specific humidity H ₂ ¹⁸ O	Qair18 ^b	kg kg ⁻¹	N/A
Specific humidity HDO	QairD ^b	kg kg ⁻¹	N/A
Large-scale snow H ₂ ¹⁶ O	SNOWL16 ^b	kg m ⁻² s ⁻¹	Downward
Large-scale snow H ₂ ¹⁸ O	SNOWL18 ^b	kg m ⁻² s ⁻¹	Downward
Large-scale snow HDO	SNOWLD ^b	kg m ⁻² s ⁻¹	Downward
Convective snow H ₂ ¹⁶ O	SNOWC16 ^b	kg m ⁻² s ⁻¹	Downward
Convective snow H ₂ ¹⁸ O	SNOWC18 ^b	kg m ⁻² s ⁻¹	Downward
Convective snow HDO	SNOWCD ^b	kg m ⁻² s ⁻¹	Downward

ALMA does not use so many solar radiation categories, NCEP reanalysis names used instead.

N.B. D is used in variable names instead of ²H.

^a ALMA has two sign conventions: we adopt the first here ('traditional').

^b ALMA does not have an isotope convention, new conventions suggested.

^c Bottom level=the lowest atmospheric level in REMOiso, set at Sigma level=0.9922814815.

a length of 4 yr and a timestep of 15 min. If any ILSS operated at a different temporal resolution, the forcing data was either averaged or interpolated. The forcing data from REMOiso were checked, as far as possible, against NCEP reanalysis data and hourly discontinuities were noticed in the radiation data. To remove these, the downward short-wave and long-wave radiation were smoothed using a uniform weighted filter with a window width of 2 h.

Table 2
ILSS variables generated in the iPILPS Phase 1 simulations

Model outputs	iPILPS		
Definition	ALMA		
	Name	Units	+ Sign
Evapotranspiration amount (total)	Evap	kg m ⁻² s ⁻¹	Upward
Root zone ^a drainage	Qrz ^c	kg m ⁻² s ⁻¹	Out of grid cell
Snow melt	Qsm	kg m ⁻² s ⁻¹	Solid to liquid
Total interception storage on the canopy	CanopInt	kg m ⁻²	N/A
Total root zone soil water	Rootmoist	kg m ⁻²	N/A
Soil moisture (liquid or frozen) in each of all soil layers ^b	Soilmoist	kg m ⁻²	N/A
Snow pack	SWE	kg m ⁻²	N/A
Effective radiative temperature	RadT	K	N/A
Canopy temperature, if present	VegT	K	N/A
Depth averaged temperature for each of all soil layers	SoilTemp	K	N/A
Depth averaged temperature for the root zone	RzT ^c	K	N/A
Absorbed solar radiation	Qg	W m ⁻²	Downward
Net radiation	Xnet	W m ⁻²	Downward
(Incoming solar radiation)–(outgoing SW radiation)	Swnet	W m ⁻²	Downward
(Incident LW radiation)–(outgoing LW radiation)	Lwnet	W m ⁻²	Downward
Latent heat flux	Qle	W m ⁻²	Upward
Sensible heat flux	Qh	W m ⁻²	Upward
Surface albedo	Albedo	%	N/A
Canopy transpiration	Tveg	kg m ⁻² s ⁻¹	Upward
Canopy evaporation	Ecanop	kg m ⁻² s ⁻¹	Upward
Ground evaporation	Esoil	kg m ⁻² s ⁻¹	Upward
Soil water (in each of all soil layers)	H2OSOI ^c	kg m ⁻²	N/A
H ₂ ¹⁸ O water (in each of all soil layers)	H18SOI ^c	kg m ⁻²	N/A
HDO water (in each of all soil layers)	HDOSOI ^c	kg m ⁻²	N/A
H ₂ ¹⁸ O canopy vapour	RCANV18 ^c	mol mol ⁻¹	N/A
HDO canopy vapour	RCANVD ^c	mol mol ⁻¹	N/A
H ₂ ¹⁸ O canopy transpiration	QVEGT18 ^c	kg m ⁻² s ⁻¹	Upward
HDO canopy transpiration	QVEGTD ^c	kg m ⁻² s ⁻¹	Upward
H ₂ ¹⁸ O canopy evaporation	QVEGE18 ^c	kg m ⁻² s ⁻¹	Upward
HDO canopy evaporation	QVEGED ^c	kg m ⁻² s ⁻¹	Upward
H ₂ ¹⁸ O ground evaporation	QSOIL18 ^c	kg m ⁻² s ⁻¹	Upward
HDO ground evaporation	QSOILD ^c	kg m ⁻² s ⁻¹	Upward
Surface runoff	Qs	kg m ⁻² s ⁻¹	Out of grid cell
H ₂ ¹⁸ O surface runoff	Qs18 ^a	kg m ⁻² s ⁻¹	Out of grid cell
HDO surface runoff	QsD ^c	kg m ⁻² s ⁻¹	Out of grid cell
Subsurface runoff (in each of all soil layers)	Qsb	kg m ⁻² s ⁻¹	Out of grid cell
H ₂ ¹⁸ O subsurface runoff (in each of all soil layers)	Qsb18 ^c	kg m ⁻² s ⁻¹	Out of grid cell
HDO subsurface runoff (in each of all soil layers)	QsbD ^c	kg m ⁻² s ⁻¹	Out of grid cell

^a 'Root zone' in ALMA is the soil layer that its moisture is available for transpiration.

^b The number and depth of all soil layers used in the ILSS are required.

^c New ALMA variables (N.B. D is used in variable names instead of ²H).

Unfortunately, we could not obtain separate streams of direct and diffuse solar radiation at the surface nor the visual (VIS) and near-infrared (NIR) proportions of the downward short-wave radiation from REMOiso. For the VIS/NIR, we used a 50:50 split of downward short-wave radiation. In the absence of information from REMOiso on the partitioning between diffuse and direct irradiance, we elected to divide the global irradiance as 30% diffuse and 70% direct for all three locations. This approximation seems justified since under clear skies diffuse radiation comprises around 10% of the global

irradiance, while, even for very cloud locations such as the Antarctic coast, the fraction of total global irradiance present as diffuse radiation is less than 50%. Although this strategy limits the evaluation of aspects of simulated space (notably 100% diffuse under completely cloudy skies), it seemed prudent in this first phase of iPILPS to avoid the introduction of another set of variables and parameters associated with empirical schemes for derivation of diffuse and direct irradiance. The authors are aware of the inadequacy of this assumption when the accurate estimation of diffuse radiation is important, but

Table 3

(a) Soil and (b) vegetation parameters used in iPILPS Phase 1 numerical experiments for Manaus, Munich and Tumbaramba

(a)												
Location	Ecotype and climate	Annual mean air temperature (K)	Soil particle size			Soil albedos						
			% Sand	% Silt	% Clay	Dry VIS	Dry NIR	Wet VIS	Wet NIR			
Manaus	Tropical rainforest	300	43.6	19.0	37.4	0.18	0.36	0.09	0.18			
Munich	Mid-lat. deciduous woodland	281	31.2	38.8	30.0	0.18	0.36	0.09	0.18			
Tumbarumba	Eucalypt woodland	285	48.0	28.0	24.0	0.12	0.24	0.06	0.12			

(b)												
	Jan	February	March	April	May	June	July	August	September	October	November	December
<i>Manaus</i>												
FVC ^a	0.90	0.90	0.90	0.90	0.90	0.90	0.90	0.90	0.90	0.90	0.90	0.90
LAI ^b	5.01	5.01	5.01	5.01	5.01	5.01	5.01	5.01	5.01	5.01	5.01	5.01
<i>Munich</i>												
FVC	0.90	0.90	0.90	0.90	0.90	0.90	0.90	0.90	0.90	0.90	0.90	0.90
LAI	5.00	5.00	5.00	5.00	5.00	5.00	5.00	5.00	5.00	5.00	5.00	5.00
<i>Tumbarumba</i>												
FVC	0.45	0.45	0.45	0.45	0.45	0.45	0.45	0.45	0.45	0.45	0.45	0.45
LAI	1.40	1.40	1.40	1.40	1.40	1.40	1.40	1.40	1.40	1.40	1.40	1.40

The ecotypes and mean annual air temperature of the sites are also included.

^a Fractional vegetation cover.

^b Leaf area index.

only one ILSS (C) required these extra radiation variables. Improvements to the derivation of extra radiation forcing will be made in future iPILPS experiments.

The above experimental plan was not followed for the model labelled Model E (in this document), which reported results from online GCM experiments which were fully enabled with isotopic tracers. Several years of output for the variables in Table 3 were obtained from these online runs (using 365-day years) for the three experimental locations. Hence, the forcing for the ILSS E was different from the prescribed iPILPS forcing data. The resulting differences are discussed further below.

Although BC24 simulations were submitted and are available on the iPILPS web, this paper, in line with the Workshop, focuses exclusively on the equilibration year: EQY1.

3. Intercomparison of iPILPS simulations

The Workshop established its goals as: to demonstrate that isotopically enabled land-surface schemes (ILSSs) generate plausible simulations at the diurnal scale of the exchanges of stable water isotopes (SWIs) at the soil, plant, air interfaces or to identify their

shortcomings and propose ways of improving the simulations. The specific questions for discussion at the iPILPS Workshop were:

- Are simulation differences due to (1) sensitivity to forcing, (2) parameterization differences, (3) both?
- Is the [Craig and Gordon \(1965\)](#) isotope evaporation model ‘adequate’ for use in ILSSs and, if not, what is required? and
- On diurnal scales how large are SWI differences; what observations could illuminate ‘adequacy’?

It was quickly determined that there is little, or no, point in analysing SWI simulation results if the ILSSs are inadequate from the point of view of: (1) conservation of energy and water, and (2) adequacy of the gross fluxes of energy and water. We therefore reviewed these first using methods developed in PILPS (e.g. [Chen et al., 1997](#)). Although some energy and moisture balance problems remain in ILSSs B and C ([Figs. 1 and 2](#)), several variables for these ILSSs have been plotted, simply for comparison purposes. Given the remaining errors, the simulation outputs of these ILSSs must be currently interpreted carefully. Many participants have found this intercomparison project to

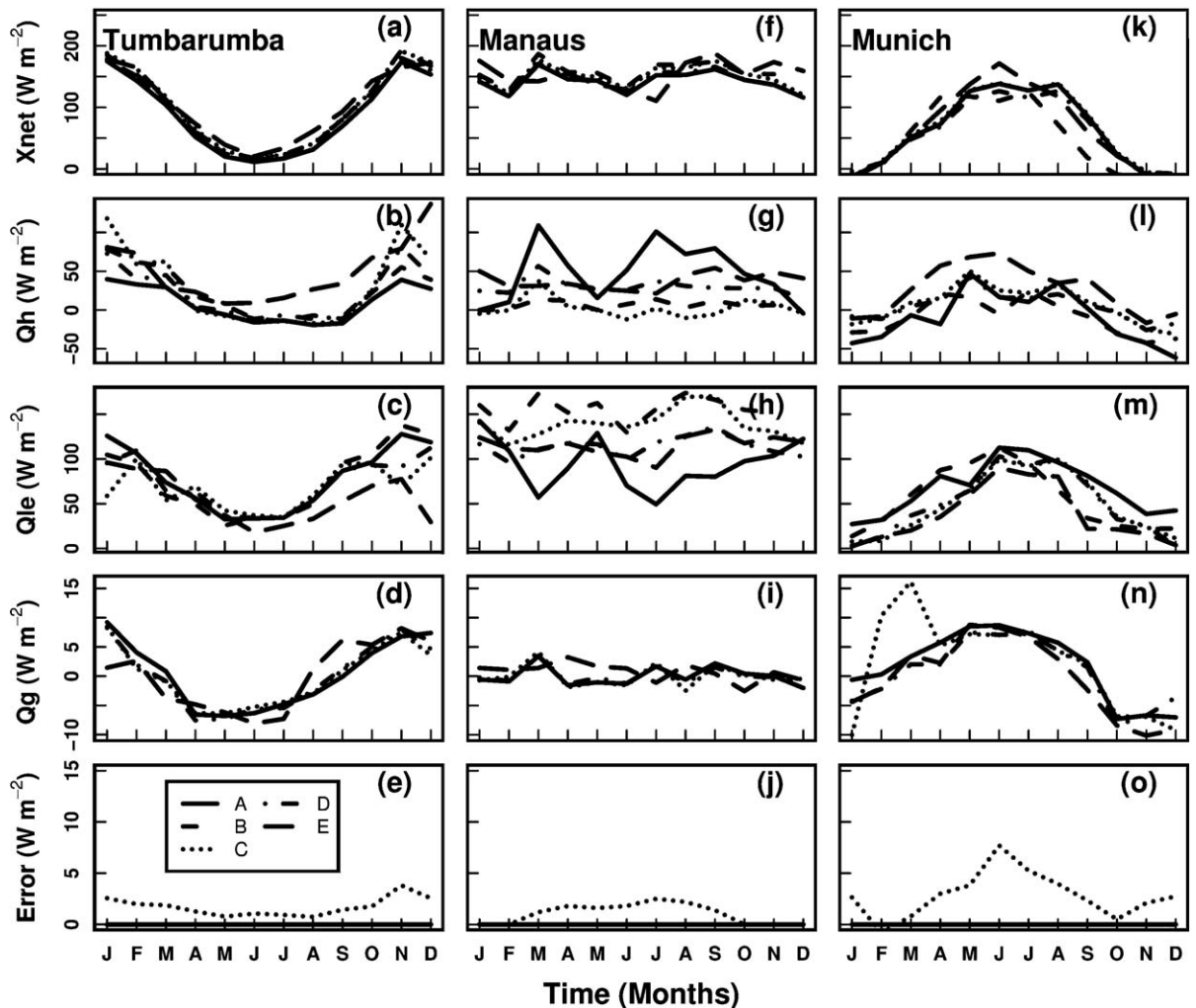


Fig. 1. Components of the monthly surface energy budget. (a,f,k) X_{net} =net radiative flux, (b,g,l) Q_{h} =sensible heat flux, (c,h,m) Q_{le} =latent heat flux, (d,i,n) Q_{g} =heat flux into ground, (e,j,o) energy imbalance (or error= $X_{\text{net}}-Q_{\text{h}}-Q_{\text{le}}-Q_{\text{g}}$) all in W m^{-2} for the final year of the equilibration simulation, EQY1, for Tumbarumba, Manaus and Munich. ILSSs are designated by letter and line type.

be a valuable exercise and, as a result, the participants have been or currently are, working to improve their models in many areas, including conservation (discussed below).

3.1. Energy and gross water simulations for EQY1

In the following sections, the overall conservation in the annual energy and water budgets is examined, as well as variations on monthly and diurnal timescales. Secondly, the effect of model complexity on the annual budgets is explored using the ‘‘PILPS plot’’ developed during the early PILPS experiments. Thirdly, isotopic fluxes at monthly and diurnal timescales are investigated, and a new graphic representation is introduced for the iPILPS model intercomparison.

3.1.1. Conservation

3.1.1.1. Annual. Outputs from all schemes were checked to ensure the conservation of bulk energy and water over the equilibrium year. ILSSs A, B, D and E all have annual means of energy and water fluxes such that:

$$|X_{\text{net}}-Q_{\text{le}}-Q_{\text{h}}| < 0.3 \text{ W m}^{-2} \quad (1)$$

$$|\text{Pr}-\text{Evap}-\text{Ro}| < 3 \text{ kg m}^{-2} \text{ yr}^{-1} \quad (2)$$

where X_{net} is net radiation (W m^{-2}), Q_{le} is latent heat (W m^{-2}), Q_{h} is sensible heat (W m^{-2}), Pr is precipitation ($\text{kg m}^{-2} \text{ yr}^{-1}$), Evap is total evapotranspiration ($\text{kg m}^{-2} \text{ yr}^{-1}$) and Ro is surface + subsurface runoff ($\text{kg m}^{-2} \text{ yr}^{-1}$). (Note that we use Table 2 radiation variable names but prefer the

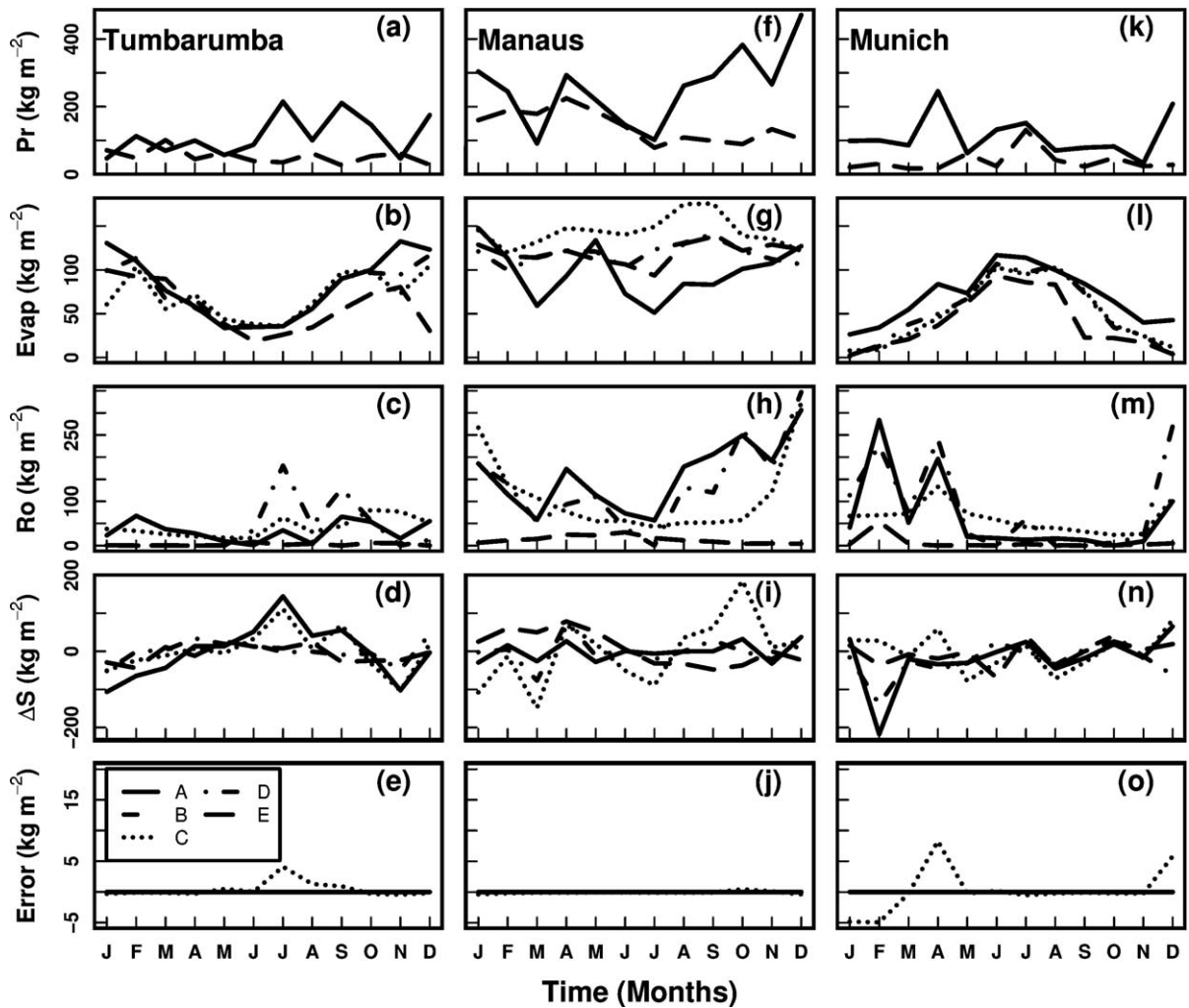


Fig. 2. Components of the monthly water budget (a,f,k) Pr=total precipitation, (b,g,l) Evap=total evapotranspiration, (c,h,m) Ro=total runoff, (d,i,n) ΔS=total change in stored water (canopy, soil, snow), (e) water imbalance (or error=Pr–Evap–Ro–ΔS) all in kg m⁻² month⁻¹ for the final year of the equilibration simulation, EQY1, for Tumbarumba, Munich and Manaus. ILSSs are designated by letter and line type. Note that models A–D are forced with the same precipitation data.

simpler terms for the water variables throughout the text.) Note that the energy of precipitation is included in the Table 2 forcing variables, but we have neglected it in Eq. (1), as in previous PILPS experiments (e.g. Chen et al., 1997) because its value is small. The conservation threshold for the surface water budget is selected to be approximately equivalent to that for energy budget, based on the water–energy relationship through the latent heat of vaporization.

3.1.1.2. Monthly. Similarly, outputs from all schemes were checked to ensure the conservation of bulk energy and water over months in the equilibrium year, EQY1.

The expected monthly surface energy balance is:

$$X_{netj} - Q_{le_j} - Q_{h_j} - Q_{g_j} = 0 \quad (3)$$

where j is the month index and Q_g is the sum of the heat flux into the soil, canopy and snowpack. Because the canopy heat capacity is small, the vegetation heat flux can be ignored here.

The expected monthly water balance is:

$$Pr_j - Evap_j - Ro_j - \Delta S_j = 0 \quad (4)$$

where ΔS_j is the change in the total storage water (soil, canopy and snowpack) for month j .

Figs. 1 and 2 show the components of the energy and water budgets, for the five ILSSs, at a monthly timescale

(these diagrams also show the seasonal cycle, discussed further below). The monthly energy budget (Fig. 1) errors are $<|0.3| \text{ W m}^{-2}$ for four models, but $<|15| \text{ W m}^{-2}$ for C (some steps have been taken to correct this). The monthly water budget (Fig. 2) errors are generally $<|0.25| \text{ kg m}^{-2} \text{ month}^{-1}$. Model B is not included in the diagrams showing the runoff and evaporation variables because of inconsistencies in its output files. Evaporation in particular needed to be scaled by a fitting factor to be in the same order of magnitude as other components of the water budget. This requirement was traced to a bug in the code, relating to a missing time weighing factor in the output routine of this accumulated variable. Even this improvement is not sufficient to achieve the closure of ILSS B's water budget. Further investigation reveals that the incorrect evaporation fluxes are related to a diagnostic error, which does not significantly affect the soil water prognosis.

3.1.2. Annual means and seasonal cycles

This paper examines only the differences between the models, rather than differences between the models and observational data. This is, in part, because of the climatological nature of the REMOiso forcing, and hence of the simulation and, in part, because of the lack of high temporal resolution observations.

The statistics for the components of annual energy and water budgets of the models are shown in Table 4 (note that all the models are used in calculating the median, minimum and maximum values below, but the median effectively moderates the importance of the most “outlying” model). For Tumbarumba, the “median model” (that is, the median values from the five ILSSs) partitions $\sim 96 \text{ W m}^{-2}$ of net radiation into $\sim 15 \text{ W m}^{-2}$ of sensible heat and $\sim 76 \text{ W m}^{-2}$ of latent energy (note that the partitioning does not necessarily sum to the available energy due to partly the use of medians and partly because of non-closure of surface energy balance by the ILSSs). For Manaus, the “median model” partitions $\sim 151 \text{ W m}^{-2}$ of net radiation into $\sim 28 \text{ W m}^{-2}$ of sensible heat and $\sim 118 \text{ W m}^{-2}$ of latent energy. For Munich, the “median model” partitions $\sim 58 \text{ W m}^{-2}$ of net radiation into $\sim 6 \text{ W m}^{-2}$ of sensible heat and $\sim 43 \text{ W m}^{-2}$ of latent energy. More importantly, the intermodel variation in the sensible and latent heat values is large. The variation, shown as the total range, for sensible heat flux is $\sim 24, 49$ and 43 W m^{-2} , and for latent heat flux is $27, 62$ and 45 W m^{-2} for Tumbarumba, Manaus and Munich, respectively.

The median annual water budgets are as follows. For Tumbarumba, the “median model” partitions $\sim 100 \text{ kg m}^{-2} \text{ month}^{-1}$ of precipitation into $\sim 19 \text{ kg m}^{-2}$

Table 4

The minimum, median and maximum values of land-surface variables from five ILSSs for the equilibrium year (EQY1) for three locations

Site	Variable	Units	Median	Min	Max
Tumbar	Xnet	W m^{-2}	96	87	102
	Qh	W m^{-2}	15	8	32
	Qle	W m^{-2}	76	54	80
	Qg	W m^{-2}	0	0	1
	Pr	$\text{kg m}^{-2} \text{ month}^{-1}$	100	51	100
	Evap	$\text{kg m}^{-2} \text{ month}^{-1}$	73	56	83
	Ro	$\text{kg m}^{-2} \text{ month}^{-1}$	19	1	36
	ΔS	$\text{kg m}^{-2} \text{ month}^{-1}$	0	-7	5
	Manaus	Xnet	W m^{-2}	151	144
Qh		W m^{-2}	28	0	49
Qle		W m^{-2}	118	94	156
Qg		W m^{-2}	0	-1	1
Pr		$\text{kg m}^{-2} \text{ month}^{-1}$	264	137	264
Evap		$\text{kg m}^{-2} \text{ month}^{-1}$	121	97	142
Ro		$\text{kg m}^{-2} \text{ month}^{-1}$	96	12	176
ΔS		$\text{kg m}^{-2} \text{ month}^{-1}$	0	-2	15
Munich		Xnet	W m^{-2}	58	40
	Qh	W m^{-2}	6	-12	31
	Qle	W m^{-2}	43	22	66
	Qg	W m^{-2}	2	0	5
	Pr	$\text{kg m}^{-2} \text{ month}^{-1}$	93	26	93
	Evap	$\text{kg m}^{-2} \text{ month}^{-1}$	42	23	69
	Ro	$\text{kg m}^{-2} \text{ month}^{-1}$	31	2	63
	ΔS	$\text{kg m}^{-2} \text{ month}^{-1}$	0	-3	3

The values are derived from the unweighted average value of all months.

month^{-1} of runoff and $\sim 73 \text{ kg m}^{-2} \text{ month}^{-1}$ of evaporation. For Manaus, the “median model” partitions $\sim 264 \text{ kg m}^{-2} \text{ month}^{-1}$ of precipitation into $\sim 96 \text{ kg m}^{-2} \text{ month}^{-1}$ of runoff and $\sim 121 \text{ kg m}^{-2} \text{ month}^{-1}$ of evaporation. For Munich, the “median model” partitions $\sim 93 \text{ kg m}^{-2} \text{ month}^{-1}$ of precipitation into $\sim 31 \text{ kg m}^{-2} \text{ month}^{-1}$ of runoff and $\sim 42 \text{ kg m}^{-2} \text{ month}^{-1}$ of evaporation. Again, more importantly, the variation between the models in the evaporation and runoff is large. This variation or total range (among the different ILSSs) is $>25, >45$ and $>45 \text{ kg m}^{-2} \text{ month}^{-1}$ for Tumbarumba, Manaus and Munich, respectively. The largest variations here are because Model E was run online, and hence received its forcing data from the atmospheric module of a GCM, different from REMOiso. This is evident in Fig. 1(k), where Model E shows a seasonal cycle of the surface net radiation different from other models mainly because of different regimes of solar radiation incident at the surface.

Comparing the values reported for Qle and Evap in Table 4 reveals an inconsistency in the models' outputs. For example, in the absence of snow/ice cover (e.g. Manaus), the relationship $Qle = \lambda \times \text{Evap}$ holds, where λ the latent heat of vaporization is about $25. \text{e}5 \text{ J kg}^{-1}$ at $0 \text{ }^\circ\text{C}$. Therefore, taking the maximum Evap of

142 kg m⁻² month⁻¹ for Manaus, the maximum Q_{le} should not exceed 135 W m⁻², much smaller than the 156 W m⁻² reported by the ILSSs. Such intermodel variation is due to either (i) model behaviour, (ii) unresolved errors in reporting model output or (iii) both. There is no doubt that three ILSSs meet the energy balance criteria (and have been reported in the desired way: A, D and E, Fig. 1 is proof of this). Any remaining problems with the ILSSs can only be solved by individual model owners (with the help of the iPILPS team).

The seasonal cycles can also be seen in Figs. 1 and 2. The expected seasonal cycles are replicated for Munich and Tumbaramba. The expected increase in runoff in the Manaus wet season (December–February) is also shown by all models except E, probably due to the very different seasonal cycle of precipitation used by E (see Fig. 2a).

3.1.3. Diurnal cycles

Figs. 3–8 show the components of the energy and water budgets, for the five ILSSs, with hourly resolution constructed by averaging all the days in January and July (again, the five models are designated by letter and line type).

3.1.3.1. Energy budget. The shape of the diurnal cycle of the net radiation is generally similar for each model (but different between the locations). More noticeably, the variation between different models is of the order of 10¹–10² W m⁻². The variation in the main components of net radiation (that is, sensible and latent heat fluxes) is as large or even larger. Similar to the case of seasonal cycle, Model E simulates the diurnal cycle of net radiation differently from the other models. Compared to other ILSSs, E simulates the highest daytime surface net radiation in January and lowest in July, with a tendency of losing more surface energy at night (Fig. 3a,e). Given the similar solar zenith angles for January and July in Manaus, one expects that the diurnal cycles of net radiation be similar for the 2 months. This is correct for the four ILSSs forced by REMOiso, but the coupled Model E shows the diurnal cycles of net radiation for the two days that are too different in magnitude to be correct for a site close to the Equator.

The partitioning of the surface net radiation between Q_h and Q_{le} in the 2 months is very different for Model A, which shows much lower Q_{le} and higher Q_h than other models in July. This could be the

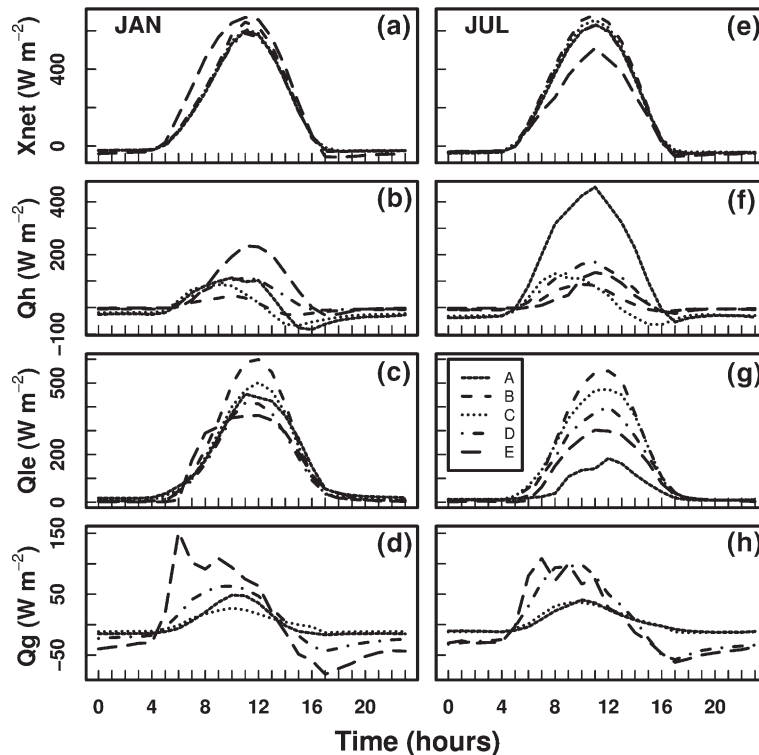


Fig. 3. Components of the diurnal surface energy budget for January (left) and July (right) created by averaging all 30 days in each month. (a,e) X_{net}=net radiative flux, (b,f) Q_h=sensible heat flux, (c,g) Q_{le}=latent heat flux, (d,h) Q_g=heat flux into ground, all in W m⁻² for the final year of the equilibration simulation, EQY1, for Manaus. ILSSs are designated by letter and line type.

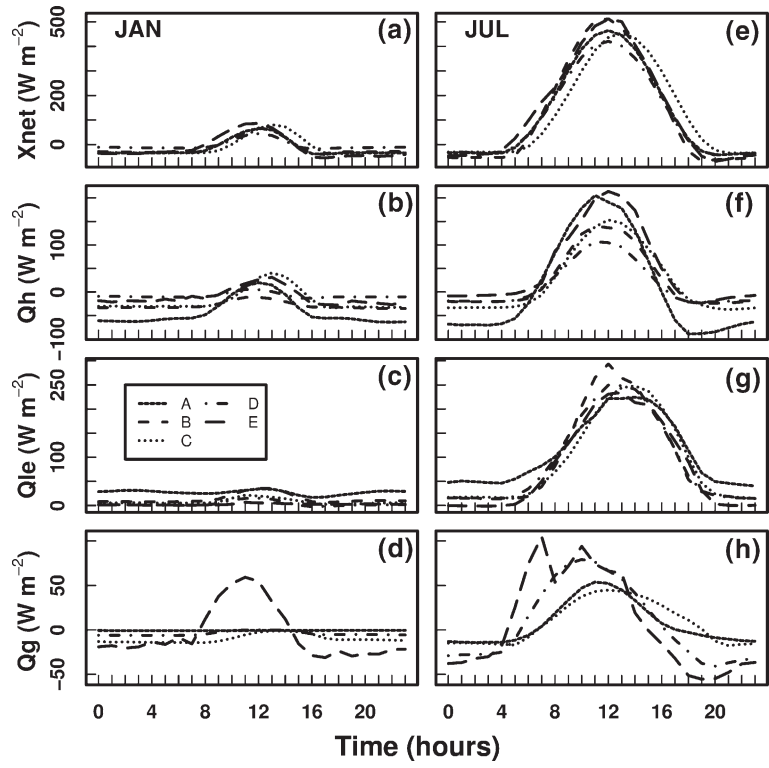


Fig. 4. As in Fig. 3, but for Munich.

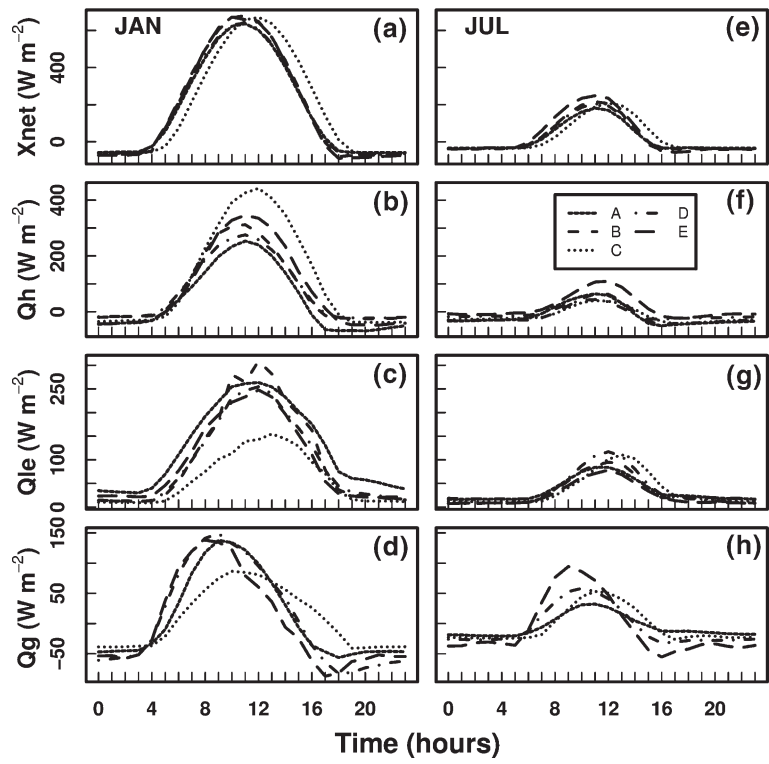


Fig. 5. As in Fig. 3, but for Tumbarumba.

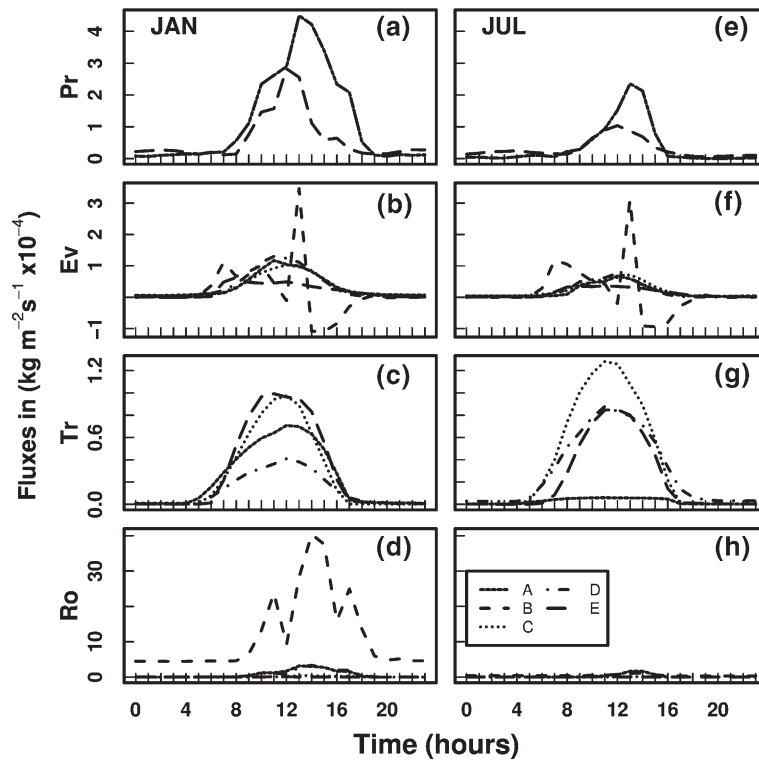


Fig. 6. Components of the diurnal water budget for January (left) and July (right) created by averaging all 30 days in each month. (a,e) Pr=precipitation, (b,f) Ev=(soil+canopy) evaporation, (c,g) Tr=transpiration, (d,h) Ro=total (surface+subsurface) runoff, all in kg m^{-2} for the final year of the equilibration simulation, EQY1, for Manaus. ILSSs are designated by letter and line type.

result of oversensitivity of A's evaporation to precipitation, problem with transpiration modelling (see Fig. 6(g)) or errors in output files. Model A also simulates too high sensible heat flux from the atmosphere to the surface and too high latent heat flux from the surface during the night in July and throughout the day in January in Munich (Fig. 4). Considering the fact that air temperature and humidity for the simulations are prescribed (by REMOiso), such results should arise from Model A having a too low surface temperature and too high surface air humidity (a function of surface available moisture and surface temperature—in contradiction with the expected low temperature). It also might be that A has a problem of too little resistance to boundary layer fluxes, when the atmosphere is in stable conditions (during nights and the cold season). In Model C, for Tumburumba, the latent heat flux on an average January day is $\sim 100 \text{ W m}^{-2}$ less than the other models (Fig. 5). The phase of the energy components also differs widely between the different models. For example, the peaks in latent heat and ground heat flux generally occur earlier in Models E and D than C, but this is not always the case (for example, Munich in January, Fig. 4). Thorough

investigation needed by the modelling groups to identify the cause(s) of these model misbehaviours. The purpose of this paper is to focus mainly on the isotope differences, and how these are linked to atmospheric forcing and model structure.

3.1.3.2. Water budget. The precipitation is the same for each model (for a particular location) because it is prescribed, except for Model E (the online GCM run). Hence, there are only two lines for precipitation in Figs. 6, 7 and 8. However, the variation in the components of the water budget on the diurnal timescale is again very large. For example, for Manaus, Models A, C and D show similar patterns of evaporation and runoff, but very different transpiration patterns (Fig. 6). The phase of transpiration also differs between the ILSSs, according to location and season. For Munich and Tumburumba, all models show very different patterns of runoff, evaporation and transpiration (Figs. 7 and 8). There does not seem to be any consistency in the models' relative behaviour at these sites: each model responds to the time-invariant surface properties and forcing data for each location in complex ways.

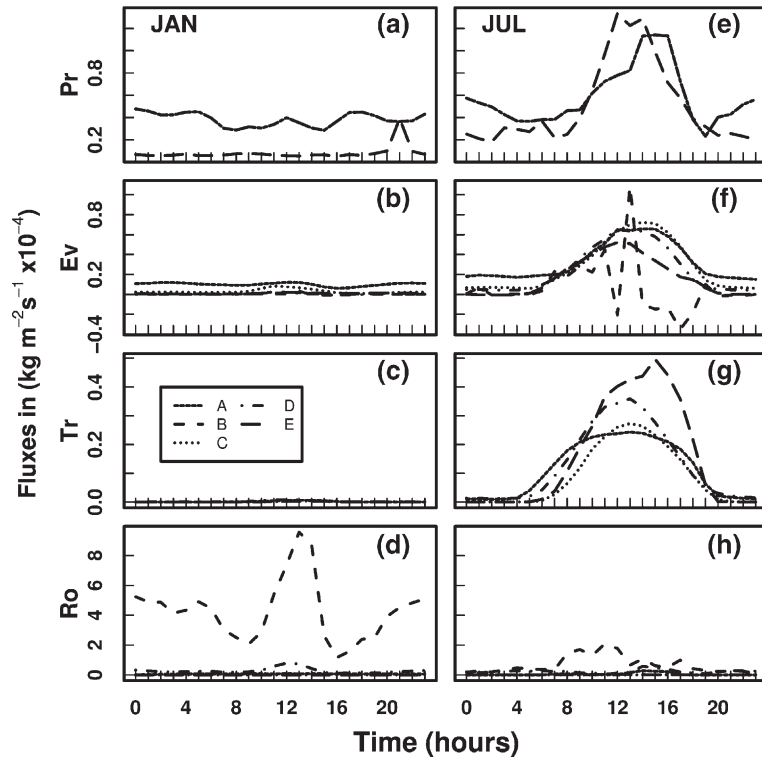


Fig. 7. As in Fig. 6, but for Munich.

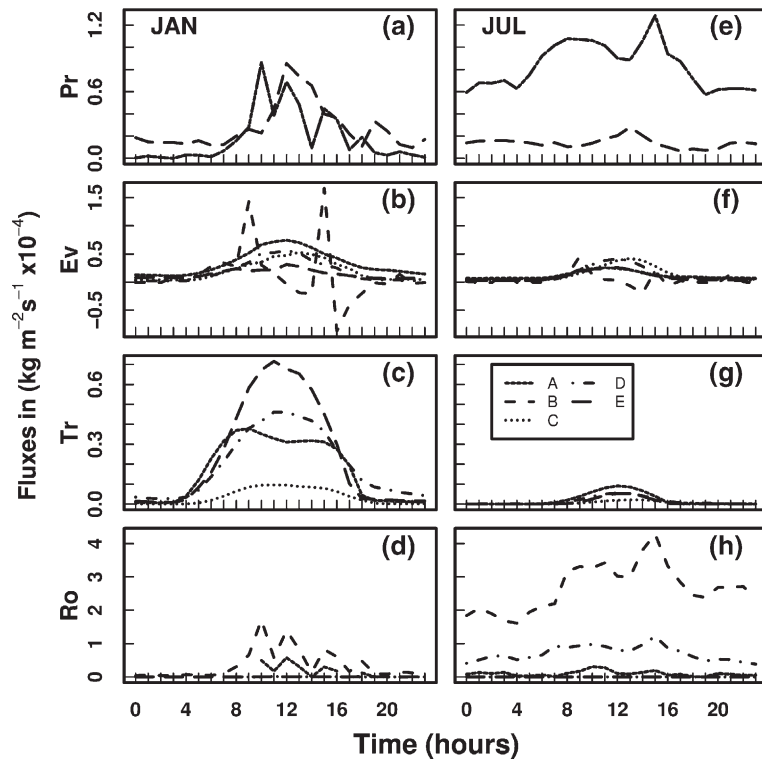


Fig. 8. As in Fig. 6, but for Tumbarumba.

3.2. PILPS plots

Fig. 9 shows the annual mean sensible and latent heat (and annual mean runoff and evaporation) plotted against each other for the five ILSSs (designated by letter; here the line type refers to the different sites: Manaus, Munich and Tumbaramba). The different models should roughly scatter along lines having a slope of -1 and have intercepts equal to the mean model net radiation ($X_{net} = Q_{le} + Q_h$). The energy graph (Fig. 9a) has been further scaled by:

$$\text{new } Q_{le}_m = Q_{le}_m(\overline{X_{net}})(X_{net}_m)^{-1} \quad (5)$$

$$\text{new } Q_h_m = Q_h_m(\overline{X_{net}})(X_{net}_m)^{-1} \quad (6)$$

where $\overline{X_{net}}$ = mean annual ($Q_{le} + Q_h$) of all models (for a particular site) and X_{net}_m = mean annual ($Q_{le} + Q_h$) for a particular model m .

This scaling is necessary because X_{net}_m is different for each model (especially E, the online GCM run). A similar scaling (but with precipitation instead of radiation) applies to the runoff/evaporation plot (Fig. 9b). The position of the ILSS letters in Fig. 9 shows the overall annual proportion of the major components that comprise the energy and moisture budgets. It is possible for two models to have a similar overall annual budget in energy or moisture, but a significant difference between the two models in how the components of the energy or moisture budget are distributed throughout the year. (These plots do not show how the energy and water is partitioned during different months through the year.)

As in the earlier PILPS analyses, the ILSSs are roughly positioned on the basis of their complexity (e.g. Henderson-Sellers et al., 2003a,b), although the number of ILSSs examined here is too small to derive a firm conclusion the Bucket land schemes follow the land-surface parameterization of Manabe (1969), while the

soil–vegetation–atmosphere transfer models (SVATs) use 1980s parameterization (for example, Sellers et al., 1986; Dickinson et al., 1986). Here, the complexity of ILSSs A, B, C, D and E corresponds to a (A) SVAT, (B) Bucket, (C) a complex SVAT, (D) SVAT/ Bucket and (E) SVAT (a complex SVAT means a third generation LSM [land-surface model], see Pitman (2003); while SVAT/ Bucket means the model is parameterized in a way that falls somewhere between these two types of parameterizations) (see also Rozenzweig and Abramopolous, 1997; Desborough, 1999; Riley et al., 2002; Takata et al., 2003). Fig. 9 shows that the ILSSs roughly plot according to their complexity. For example, ILSS E (SVAT) generally has a relatively high Q_h/Q_{le} ratio, while ILSS B (which has a Bucket hydrology) has a relatively low Q_h/Q_{le} ratio; this distribution of complexity agrees with earlier PILPS analyses (e.g. Pitman et al., 1999). ILSS D is found somewhere in the middle: it is a Bucket land scheme, but with additional bare ground and stomatal resistances. ILSSs A and C show differing behaviours between the three simulated locations (the complexity of these ILSSs makes the actual reasons for variance difficult to establish).

The patterns in the runoff/evaporation plot are less clear (Fig. 9b). The different behaviour of ILSS E is probably due to the very different rainfall forcing in the online GCM run. ILSS D generally falls between ILSS A and C, but again ILSS A and C show complex behaviour (ILSS B has been removed from this plot due to the unexplained error in its hydrology files).

4. Stable water isotope simulations for EQY1

4.1. Annual means and seasonal cycles of SWIs

Fig. 10 shows the seasonal cycles of monthly (weighted) δ values for the ^{18}O isotope (note that in

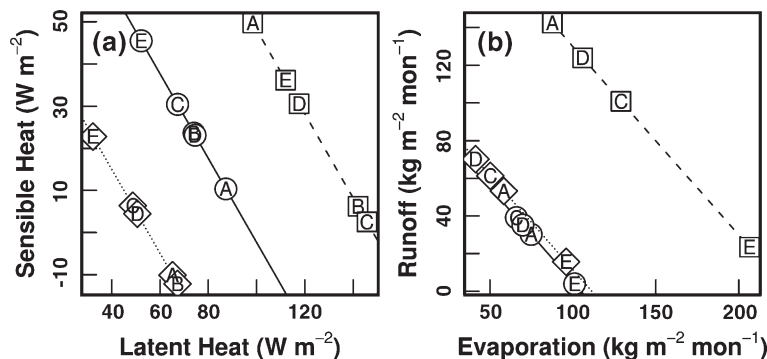


Fig. 9. Components of the annual mean surface (a) energy budget and (b) water budget. The values are scaled according to Eqs. (5) and (6). ILSSs are designated by letter. Locations are designated by symbol and line type (Manaus=square, dashed; Munich=diamond, dotted; Tumbaramba= circle, solid line). ILSS B is excluded from panel (b) because of the unexplained errors in its hydrology files.

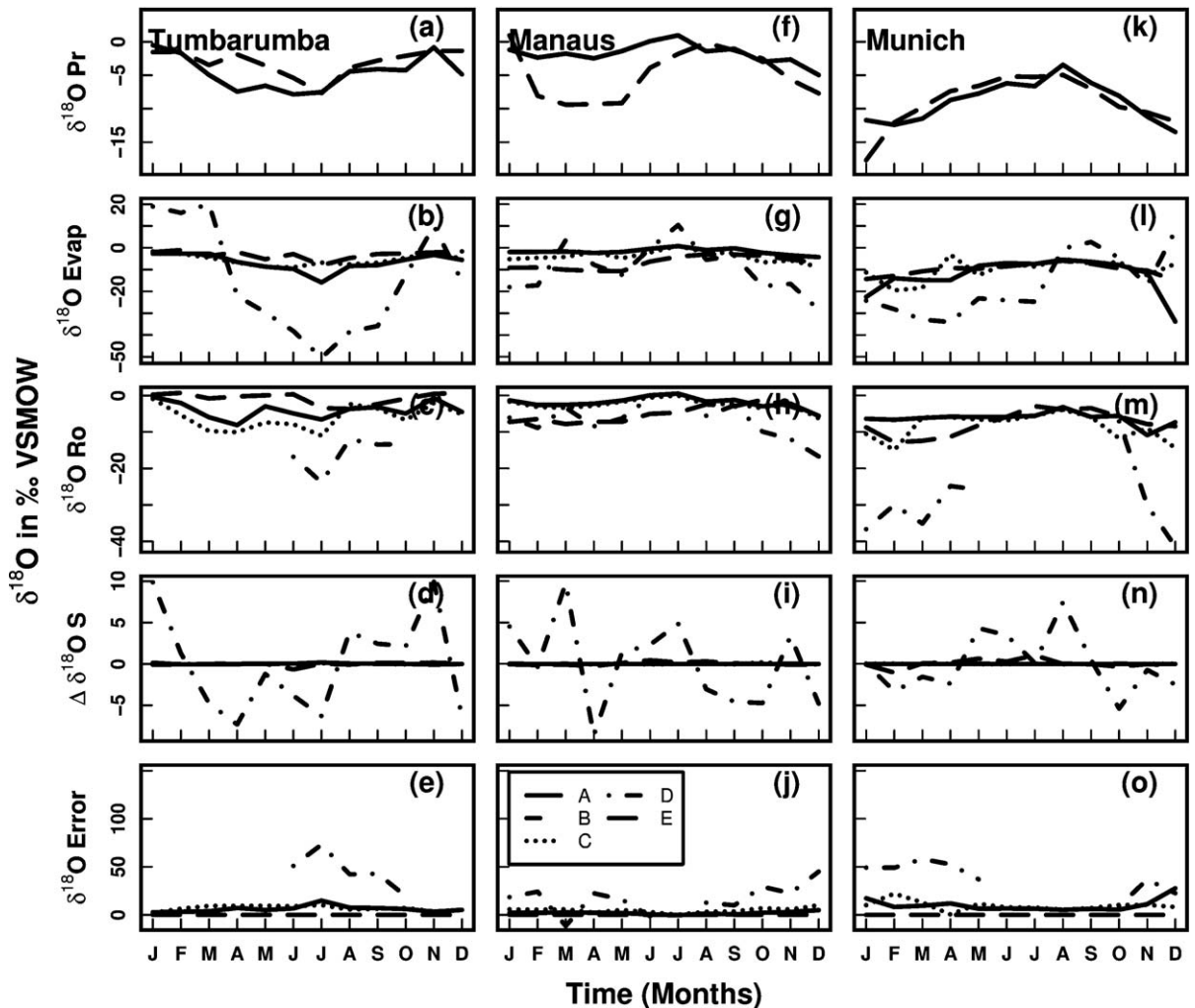


Fig. 10. Components of the monthly water isotope budget (here all δ 's refer to $\delta^{18}\text{O}$). (a,f,k) δPr =isotope ratio of total precipitation, (b,g,l) δEvap =isotope ratio of total evapotranspiration, (c,h,m) δRo =isotope ratio of total runoff, (d,i,n) $\Delta\delta\text{S}$ =total change in isotope ratio in stored water (canopy, soil, snow), (e) water isotope imbalance (or error= $\delta\text{Pr} - (\text{Evap} * \delta\text{Evap} + \text{Ro} * \delta\text{Ro} + \Delta\text{S} * \Delta\delta\text{S}) / \text{Pr}$) all relative to VSMOW for the final year of the equilibration simulation, EQY1, for Tumbarumba, Manaus and Munich. ILSSs are designated by letter and line type.

the remainder of this paper, δ without subscript refers to either isotopologue). Note that the term $\Delta\delta\text{S}$ represents the change in the isotopic content of all water storage reservoirs (snowpack, canopy and soil water) between the start and end of a month. This δ value of small water fluxes may be poorly calculated because of round-off errors but should approximate zero. However, as iPILPS did not require participants to provide isotopic information for all the reservoirs (e.g. snowpack) even though most did, any unexpected values could be due to incomplete reporting.

There are two expectations for SWIs: (1) at small intervals of time, δ runoff should equal δ precipitation, and (2) at longer timescales, variations of δ in Evap and Ro might be similar to those of Pr, because Evap and Ro

may result from a combination of multiple Pr events in previous days. On the monthly timescale, ILSSs A and C show δEvap and δRo patterns that are similar. In the case of Munich, where δPr is similar for ILSSs A–D and E, ILSSs D and E also show similar trends in δRo and δEvap , except in the summer (May–September) months when there is no runoff in ILSS D (Fig. 10). Given these similarities between the models, it is unlikely that the ILSS output diverges from the two expectations above due to inadequate structure in the models (i.e. it is very unlikely that the different schemes have been coded poorly in the same way). Some possible reasons for the similarities and differences in isotope patterns are discussed in Section 4.2. A more detailed understanding of the monthly isotope balance may be obtained by

“adding isotopes” to the monthly water balance model of Koster and Milly (1997). This will be the topic of a future paper.

4.2. Diurnal cycles of SWIs

The diurnal cycles of isotopes for the water budget components are shown in Figs. 11, 12 and 13 ($\delta^{18}\text{O}$ only). Showing the $\delta^{18}\text{O}$ for these components provides a baseline for understanding the isotope signal: the $\delta^2\text{H}$ are not shown because they are simply shifted from the $\delta^{18}\text{O}$ according to some ratio (and thus show the same monthly/diurnal pattern). However, both isotopes appear on the iPILPS website <http://ipilps.ansto.gov.au/> and the $\delta^{18}\text{O}/\delta^2\text{H}$ ratios are shown in later plots (Figs. 15–17).

Isotope values are averaged for each hour (using weighted averages) over 30 days in two different months (January and July). At this scale of aggregation, δRo values are seen not to match the precipitation (δPr). The reason for this is the selection of rainfall events, i.e. some rainfall ‘events’ are selected for infiltration, while others are selected for runoff, even at the same hour of day in a single month. This means that the weighted

isotopic composition of the rainfall and the weighted isotopic composition of the runoff, averaged at the hourly timescale over a single month, do not have to match. The same applies to longer timescales, and probably increases the disparity between simulated isotopic composition of runoff and precipitation.

This ‘event selection’ concept is also applicable to non-plant evaporation (Ev) and to transpiration (Tr). While the bulk evaporation and transpiration trends may be similar over the daily cycle, changes in the proportion of evaporation and transpiration over the daily cycle effectively changes the soil moisture depth that is being sampled. Hence, over some scale of averaging, the soil water sampled by evapotranspiration does not have to have the same isotopic composition as that of the bulk soil water (over the same depth) averaged over the same timescale. Given that, so far, all the participating ILSSs use a Craig-Gordon parameterization for evaporation, the differences in the isotopic budgets in different ILSSs is probably largely due to the selection and mixing processes. (Although the Craig and Gordon (1965) isotope evaporation model has been modified by several authors (e.g. Gonfiantini, 1986; Mathieu and Bariac, 1996), the use of modified equations in ILSS sensitivity

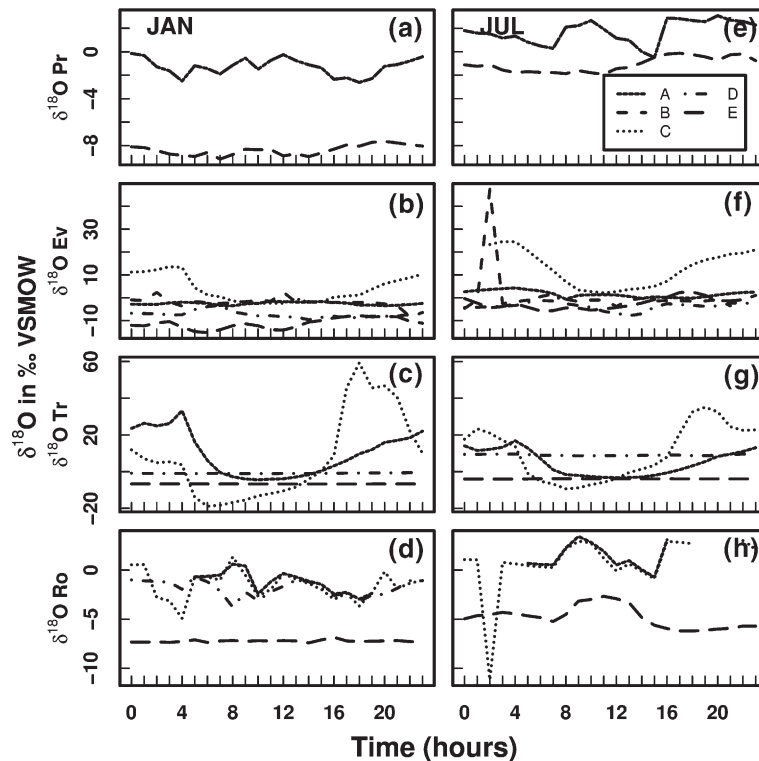


Fig. 11. Components of the diurnal water isotope budget (here all δ 's refer to $\delta^{18}\text{O}$). (a,e) δPr =isotope ratio of precipitation, (b,f) δEv =isotope ratio of evaporation (soil+canopy), (c,g) δTr =isotope ratio of transpiration, (d,h) δRo =isotope ratio of surface+subsurface runoff, all relative to VSMOW for the final year of the equilibration simulation, EQY1, for Manaus. ILSSs are designated by letter and line type.

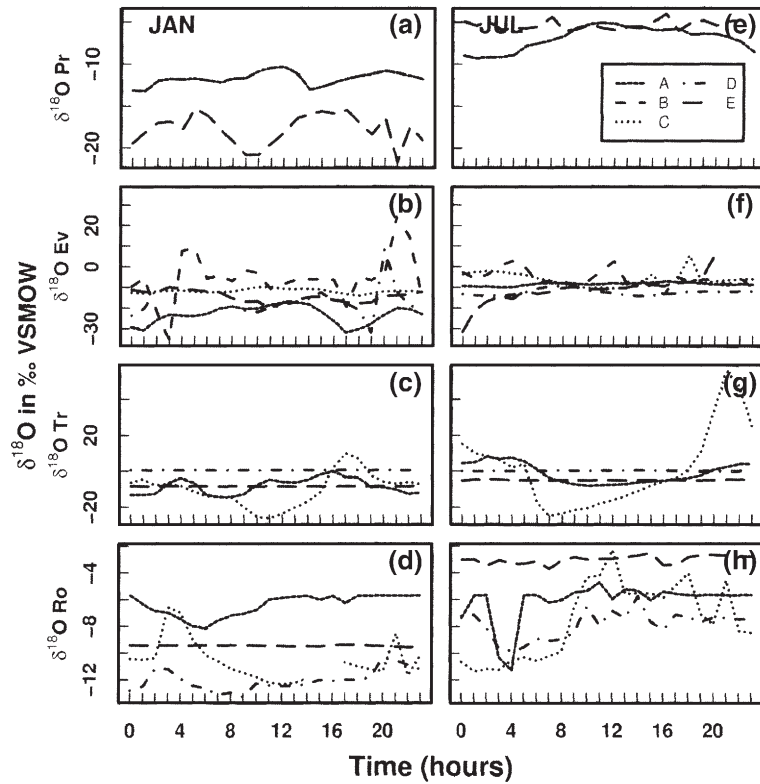


Fig. 12. As in Fig. 11, but for Munich.

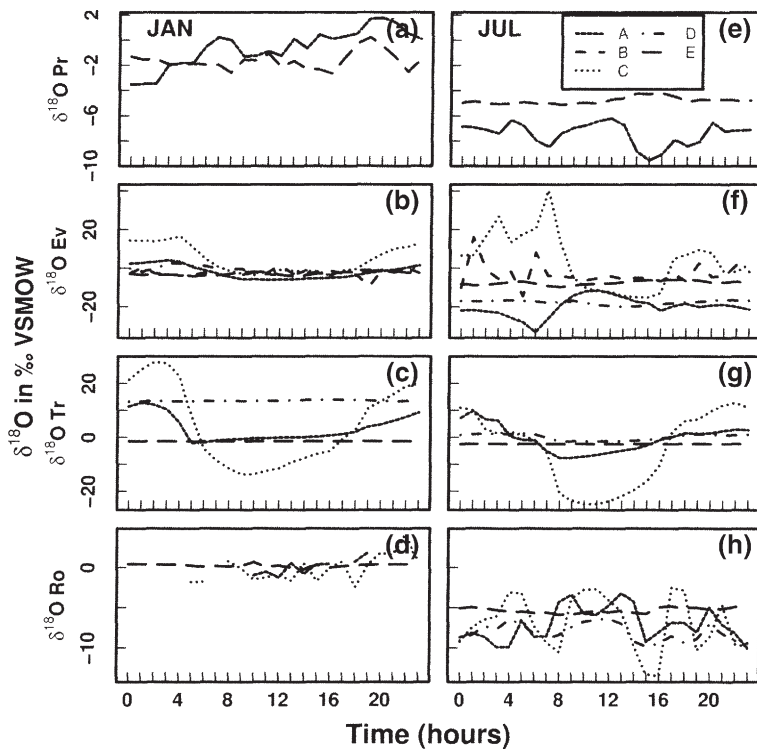


Fig. 13. As in Fig. 11, but for Tumbaramba.

has yet to be tested.) This recognition has prompted the creation of the isotope transfer function (ITF), which can be written as:

$$\delta_{\text{reservoir}} = f(\text{mixing, selection, isotope fractionation}). \quad (7)$$

That is, the δ value of a storage reservoir is a function of the selection of inputs into the reservoir, how those inputs are mixed with the reservoir and the fractionation that may occur when water is lost from the reservoir. Here, this function is discussed qualitatively, but it can be made quantitative through various statistical approaches (see below). Selection processes control which rainfall events and soil water are selected for runoff and for total evapotranspiration (Evap) and, indeed, for its components, Ev and Tr. In addition, all the land schemes have different mixing processes (i.e. how the rainfall and different soil reservoirs are mixed together when there is movement of water from one soil layer to another differs between the ILSSs). An advantage of investigating simulations by isotope-enabled land-surface schemes is that the isotopes can be used to understand the effect of these selection and mixing processes on water budgets. Although this has not been shown explicitly here, the different effects on isotopic fluxes of different mixing schemes can be seen in the ILSS papers included in this issue. One further method of analysing this might be to compare the different ILSSs by statistically fitting and plotting the convolution functions of the first two processes (mixing and selection), similar to the approach used in Weiler et al. (2003). Resulting information about the impact of parameterization choices on water budget and flux characterization cannot be easily derived from an LSS that does not have isotopic tracers.

4.3. Analysis of ILSS simulations of SWIs

This section introduces a new PILPS-style plot for the evaluation of ILSSs.

The expected monthly isotope mass balance is (to a good approximation):

$$(\delta\text{Pr}_j * \text{Pr}_j) - (\delta\text{Evap}_j * \text{Evap}_j) - (\delta\text{Ro}_j * \text{Ro}_j) - (\delta\Delta S_j * \Delta S_j) = 0 \quad (8)$$

where δPr_j is the monthly (weighted) isotope δ value of precipitation (relative to VSMOW), δEvap_j is the monthly (weighted) isotope δ value of evaporation (relative to VSMOW), δRo_j is the monthly (weighted) isotope δ value of surface plus subsurface runoff

(relative to VSMOW) and $\delta\Delta S_j$ is the monthly (weighted) isotope δ value of the change in the total storage water (relative to VSMOW). Note that, for Eq. (8), the error introduced by conversion to delta values is $<0.3\text{‰}$ over the natural range of delta values. The storage term will be zero over the entire year, for the equilibrium year (note that the year must be in isotopic equilibrium). The expected annual mass balance is then:

$$\overline{\delta\text{Pr}} = \frac{\overline{\text{Evap}}}{\overline{\text{Pr}}} \left(\frac{\sum_{\text{all } j} (\delta\text{Evap}_j * \text{Evap}_j)}{\sum_{\text{all } j} \text{Evap}_j} \right) + \frac{\overline{\text{Ro}}}{\overline{\text{Pr}}} \left(\frac{\sum_{\text{all } j} (\delta\text{Ro}_j * \text{Ro}_j)}{\sum_{\text{all } j} \text{Ro}_j} \right) \quad (9)$$

where $\overline{\delta\text{Pr}}$ is the weighted mean monthly δ precipitation value, $\overline{\text{Evap}}$ is the mean monthly evaporation, $\overline{\text{Ro}}$ is the mean monthly surface+subsurface runoff and $\overline{\text{Pr}}$ is the mean monthly precipitation.

Plotting the two terms on the right-hand side of Eq. (9) against each other generates a plot with an intercept of $\overline{\delta\text{Pr}}$ and a slope of -1 . The plot can also be scaled to take into account the situation where ILSSs are forced by rainfall with different annual $\overline{\text{Pr}}$ with the two variables scaled as follows:

$$\text{new } \delta\text{Ro}_m = \delta\text{Ro}_m \left(\frac{\overline{\delta\text{Pr}}}{\overline{\delta\text{Pr}_m}} \right) (\overline{\delta\text{Pr}_m})^{-1} \quad (10)$$

$$\text{new } \delta\text{Evap}_m = \delta\text{Evap}_m \left(\frac{\overline{\delta\text{Pr}}}{\overline{\delta\text{Pr}_m}} \right) (\overline{\delta\text{Pr}_m})^{-1} \quad (11)$$

where $\overline{\text{Pr}}$ is the mean monthly δ precipitation of all ILSSs (for a particular site) and $\overline{\delta\text{Pr}_m}$ is the weighted mean monthly δ precipitation for a particular ILSS m .

The plot for the EQY1 experiments (produced using Eq. (9), with no additional scaling) is shown in Fig. 14a for Manaus, Tumburumba and Munich (the ILSSs are designated by letters). The axes in Fig. 14a are $(\overline{\text{Evap}/\overline{\text{Pr}}})\delta\text{Evap}$ and $(\overline{\text{Ro}/\overline{\text{Pr}}})\delta\text{Ro}$. A similar plot to Fig. 9b, but produced using the mass amounts of H_2^{18}O , is shown in Fig. 14b. The axes in Fig. 14b are the scaled mass amounts of H_2^{18}O in total evaporation and runoff (the expected intercept of the lines in Fig. 14b is the mass amount of H_2^{18}O in 12-month mean precipitation). In these plots, ILSS E falls close to the line in Fig. 14b but not Fig. 14a, because although its H_2^{18}O mass is similar to that of the other models, the associated amount of H_2^{16}O is not. ILSSs A and C have similar fractionation processes in both bulk amount and isotopes in Tumburumba and Munich, but different in Manaus. In Manaus, ILSS A has more runoff (hence

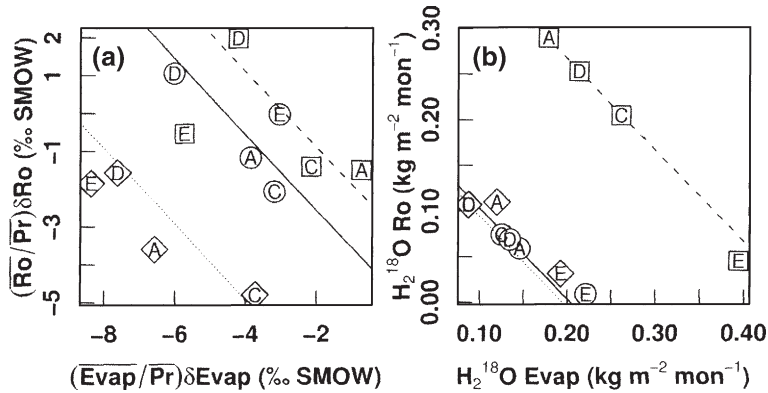


Fig. 14. Components of the annual mean water isotope budget (here all δ 's refer to $\delta^{18}\text{O}$) relative to isoflux (a) and mass (b). ILSSs are designated by letter. Locations are designated by symbols and line type (Manaus=square, dashed; Munich=diamond, dotted; Tumbaramba=circle, solid line). ILSS B is not plotted because of the unexplained errors in its hydrology files.

greater H_2^{18}O mass), but isotopic fractionation is for some reason different (since they both end up with similar weighted δ amounts for evaporation and runoff). This requires a closer investigation at the individual storm scale (beyond the scope of this paper).

Further, Fig. 14a demonstrates the intricate relationship between transpiration, soil evaporation, run-

off, rainfall event selection and their isotopic signature. It is important to note here that transpiration is generally thought to be more isotopically enriched than soil evaporation (e.g. see Gat, 1996 and also Section 4.4 below). Imagine that a single ILSS has a certain soil evaporation, transpiration and runoff partitioning. If the parameters of the evaporation and

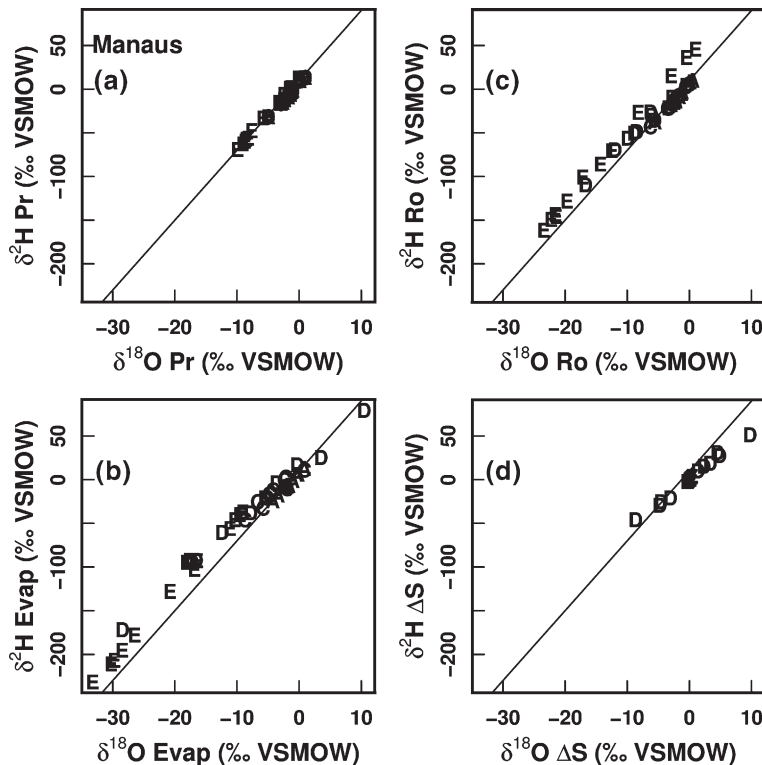


Fig. 15. Components of the twelve monthly water isotope budget, shown as a $\delta^{18}\text{O}/\delta^2\text{H}$ plot: (a) δPr =isotope ratio of total precipitation, (b) δEvap =isotope ratio of total evapotranspiration, (c) δRo =isotope ratio of total runoff, (d) $\Delta\delta\text{S}$ =isotope ratio of total change in stored water (canopy, soil, snow), all relative to VSMOW for the final year of the equilibration simulation, EQY1, for Manaus. ILSSs are designated by letter and line type. The GMWL line is the dashed diagonal.

transpiration (Tr) parameterization were changed in such a way that the total evapotranspiration (Evap) did not change, but that the Tr/Evap ratio did, then it might be expected that the δEvap signal would shift along the horizontal axis according to whether there was more or less transpiration. However, a model in isotopic equilibrium has to also shift along the site's line of equilibrium. In the case of the above scenario (where there is a change in Tr/Evap but no bulk change in Evap), the shift along the line of equilibrium can only happen if the rainfall event selection processes change in such a way that the isotopic content of the runoff (and infiltration) changes appropriately. In other words, if Tr/Evap becomes larger (with no bulk change in Evap), then the rainfall event selection processes (which partition the isotopes in runoff and infiltration) must become greater (more isotopically depleted runoff) in order to compensate for the isotopic shift due to increased transpiration. Hence, the Tr/Evap ratio is important in determining how runoff is selected from rainfall.

This apparently straightforward conclusion cannot be drawn from standard LSS analyses of runoff versus evaporation. For example, in a PILPS plot (e.g. Fig. 9), there is no indication that a change in Tr/Evap forces a change in how runoff is selected from rainfall

events. Hence, isotopes provide a new diagnostic for land surface models that is intricately related to land surface processes. Further, this new diagram (Fig. 14a) is a conceptual diagram that gives a quick summary of the annual isotope mass balance, just as the PILPS sensible and latent heat plot is a quick summary of the annual total energy budget. This new “iPILPS plot” should be a useful tool in all isotope-enabled model intercomparisons of simulations of surface–atmosphere exchanges.

4.4. $\delta^{18}\text{O}/\delta^2\text{H}$ plots

Figs. 15–17 show monthly $\delta^{18}\text{O}/\delta^2\text{H}$ plots for the components of moisture budget (ILSSs are designated by letters). The linear scatter shows that the monthly pattern of $\delta^2\text{H}$ is the same as $\delta^{18}\text{O}$. The $\delta^{18}\text{O}/\delta^2\text{H}$ ratio, however, is different between different ILSSs (except precipitation for ILSSs A–D since these all use the same, prescribed, forcing data). The precipitation from both the online GCM run (ILSS E here) and REMOiso forcing fall along the Global Meteoric Water Line, $\delta^2\text{H} = 8 * \delta^{18}\text{O} + 10$ (the GMWL is the diagonal line in Figs. 15–17). The change in the isotopic content of the storage reservoirs (snowpack, soil water and canopy water) is generally small (~ 0) for all ILSSs except D.

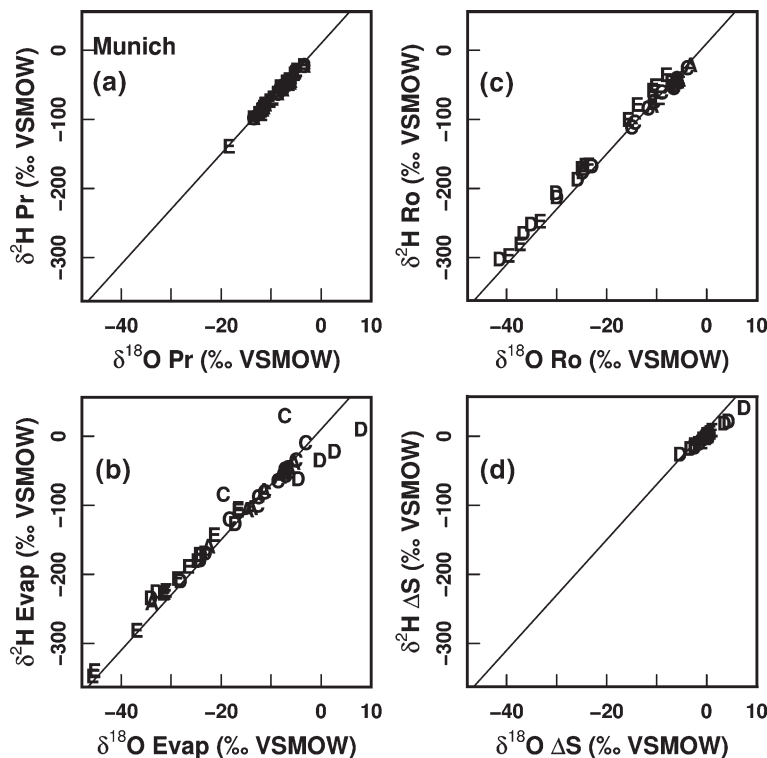


Fig. 16. As in Fig. 15, but for Munich.

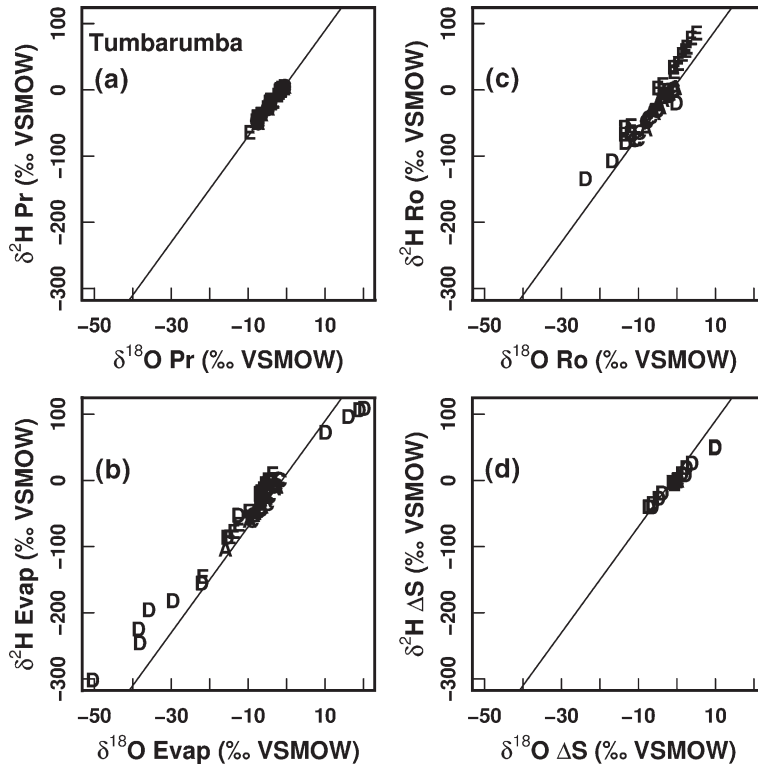


Fig. 17. As in Fig. 15, but for Tumberumba.

This suggests that for this ILSS the soil reservoir (which makes up the major component of total storage) has a very different size and residence time than the soil reservoir in the other ILSSs (which may contribute to a longer time necessary to reach isotopic equilibrium). These diagrams suggest that isotopes also have the potential to be valuable tools for learning about water residence times in land-surface schemes: features that cannot be easily achieved in LSMs without an isotopic parameterization.

The main idea behind $\delta^{18}\text{O}/\delta^2\text{H}$ plots is that evaporation should drive evaporating vapour and residual waters along a line that has a slope of <8 , because of the different transport diffusivities of $^1\text{H}_2^{18}\text{O}$ and $^1\text{H}^2\text{H}^{16}\text{O}$ (Gonfiantini, 1986). The slope of 8 is an expectation based on experimental diffusivities of the two isotopologues. The slope of the evaporation line ($\delta^{18}\text{O}/\delta^2\text{H}$) is humidity dependent, and varies from ~ 3.5 at 0% relative humidity to ~ 8 at 100%. The evaporates and residual water in the evaporating reservoir will lie along this evaporation line to the left and right of the GMWL, respectively. In Figs. 15–17, the expectation is that δ evaporation from soil and canopy interception (δEv) will fall to the left of the GMWL, since the evaporation should be isotopically

depleted, relative to the soil water and canopy-intercepted water. However, if the total evapotranspiration (plot (b)) is made up of a relatively high proportion of transpiration, then the δ evaporation (δEvap) distribution should fall closer to the GMWL, since at monthly timescales, which should approximate a steady state situation, the expectation is that δ transpiration (δTr) = δ root zone water (see Twining et al., 2006) (weighted appropriately). This is a minimalist interpretation and the situation is much more complex, even in an ILSS due to root zone isotope gradients driven by soil evaporation (these effects have yet to be properly assessed).

We can deduce that the δEvap values of ILSSs D and E appear to be more affected by soil and canopy evaporation than by transpiration. ILSSs A and C show a wide range of behaviours from place to place. For example, for C, in Manaus, δEvap is depleted relative to the GMWL, while A is not (Fig. 15). In comparison, A and C are both depleted in Tumberumba, but not to the extent of E and D (Fig. 17). Again, these behaviours cannot be easily explained without a detailed analysis of the size and residence times of the soil reservoirs, which are the source of evaporation and transpiration, and the mixing and selection processes which affect these

reservoirs (the general explanation for trends in the isotopic annual budget has been provided in Section 4.3).

In these $\delta^{18}\text{O}/\delta^2\text{H}$ plots, δ runoff may also be expected to be similar to δ precipitation because the precipitation that runs off should be unfractionated. This pattern seems to be true for ILSSs A and C, but not for D and E. From the ILSSs D and E, it appears that the rainfall that runs off is only a very small proportion of the monthly precipitation and it is also much more isotopically depleted than the weighted average monthly rainfall. Isotopic depletion in rainfall is typical of storms of long duration or high intensity, both of which fill the soil reservoir in D and E, and hence runoff would generally occur in the more isotopically depleted parts of a storm. This analysis emphasizes the value of isotopes for examining the selection processes that operate in different ILSSs and how they impact upon the feedbacks from the land surface to the atmosphere.

4.5. SWI evaluation

SWIs can be used in two distinct ways to evaluate land-surface parameterizations: (1) direct comparison of the SWI character of water stores and fluxes simulated by ILSSs with isotopic observations, and (2) comparing LSS predictions of the relative proportions of water fluxes with the proportions determined from isotopic characterization of the sources, e.g. transpired vs. non-transpired SWIs. (We note that isotopes can only be used to estimate flux partitioning if transpiration occurs at isotopic steady state (see Lai et al., 2006, p. 79), which has not yet been proven for Tumarumba.) Here, examples of both methods are given as illustrations of the power of SWIs in improving land-surface coding. The observational example comes from a preliminary

interpretation of results from the Tumarumba campaign in March 2005. Although these data have been substantially revised following recognition of operational difficulties on March 7th (Twining et al., 2006), the preliminary $\delta^2\text{H}$ values serve to illustrate the methodology.

Fig. 18 compares the $\delta^2\text{H}$ of the transpired and non-transpired moisture fluxes as predicted by the five ILSSs for March 7 of EQY1. The heavy black dashed lines are the diurnally averaged $\delta^2\text{H}$ values for these two fluxes deduced from the preliminary FTIR results using the Keeling plot method (see Henderson-Sellers, 2006). The soil evaporation has $\delta^2\text{H} \approx -95\text{‰}$, while the transpired flux has $\delta^2\text{H} \approx -40\text{‰}$. As Fig. 18 illustrates, none of the ILSSs predict $\delta^2\text{H}$ values as depleted as those deduced from the Keeling method. The ILSS (D) achieving the most depleted $\delta^2\text{H}$ values in soil plus canopy evaporation (Ev) suffers other drawbacks particularly the lack of any diurnal signal in the transpired (Tr) $\delta^2\text{H}$ combined with quite enhanced values. Interestingly, ILSSs C and D exhibit remarkably different $\delta^2\text{H}$ characteristics for these two fluxes even though they share a roughly central (i.e. “satisfactory”) position in the “PILPS plot” (Fig. 9) for Tumarumba. We have, therefore, shown that the hydrology of at least ILSS D requires further investigation on the basis of the $\delta^2\text{H}$ characterization of transpired and non-transpired evaporative fluxes.

It is possible to take preliminary FTIR data further by using the $\delta^2\text{H}$ characteristics to partition transpired and non-transpired fluxes. In the initial analysis for 7 March, a roughly 50/50 split was found (N.B. the method is yet to be fully proved). Fig. 19 illustrates how this partitioning could be applied to evaluate the gross water fluxes simulated by any LSS. If the 50/50 split was correct for 7 March as was originally believed, the five ILSSs in iPILPS could all be said to

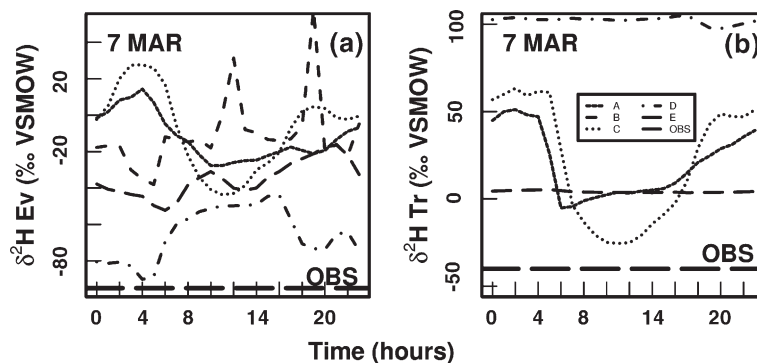


Fig. 18. Diurnal cycle of $\delta^2\text{H}$ in (a) non-transpired moisture (i.e. soil and canopy evaporation) and (b) transpiration as simulated by the five ILSSs (A–E) at Tumarumba, taken from the EQY1 for 7 March. The observations are single values (\sim diurnal means) of transpired and non-transpired flux derived from the FTIR measurements using the Keeling method.

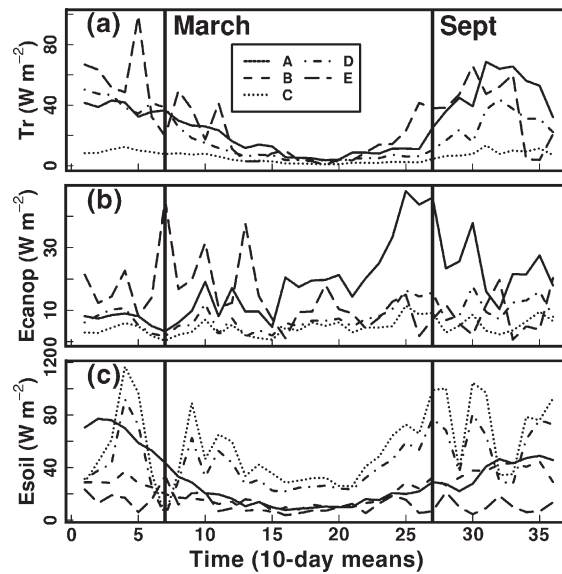


Fig. 19. Annual cycle of latent flux components (a) transpiration, (b) canopy-intercepted water evaporation and (c) soil evaporation as simulated by the five ILSSs for EQY1. The two vertical lines show the March 7 and September 28 dates. The March 7 date corresponds to 1 day during the Tumbarumba field campaign (Twining et al., 2006). The September 28 corresponds to a possible sampling day (see text).

be generating plausible proportionalities. However, if the 50/50 separation of transpired from non-transpired were actually for a spring rather than autumn day, say 28 September, then much greater difficulties are clear for some ILSSs. For example, ILSS D transpires 10 W m^{-2} , its canopy evaporation is 15 W m^{-2} , while the soil evaporation is 77 W m^{-2} , i.e. roughly a 10/90 split. In contrast, ILSS A transpires 25 W m^{-2} , has a canopy evaporation of 46 W m^{-2} and a soil evaporation of 29 W m^{-2} , giving it about a 25/75 separation. Thus, if the isotopically derived 50/50 partition were correct for either date, it would allow discrimination in September although adding little diagnostic benefit in March.

5. Summary and conclusions

The iPILPS Phase 1 experiments provide the first intercomparison of isotope-enabled land-surface schemes. Given the importance of isotope modelling in understanding the variability of both modern and palaeo-climates and the interpretation of relevant observations (e.g. Jouzel et al., 1996; Cole et al., 1999), correctly capturing the isotopic feedback between the land surface and the atmosphere is critical for appropriate analysis over a wide range of timescales. iPILPS Phase 1 has already delivered significant benefits to individual land-surface scheme owners and users in the form of improvements arising from the analyses described here.

From the experiments presented here, five main conclusions can be drawn:

- (1) In ILSSs, the partitioning of available energy and water is a function of the schemes' complexity, as was identified in early PILPS experiments. For example, ILSS B (Bucket hydrology) has a relatively high Q_{le}/Q_h ratio, while ILSS E (SVAT) has a relatively low Q_{le}/Q_h ratio.
- (2) Secondly, the isotopic equilibrium is independent of the total water and energy budget, that is, an ILSS that is in equilibrium with respect to bulk energy and water is not necessarily in isotopic equilibrium.
- (3) The isotopologues show complex responses to the hydrological parameterizations of different land-surface schemes (given the same surface properties and forcing data for a particular location). A new methodology for understanding the differences in the isotopic response of different ILSSs, the isotope transfer function (ITF), $\delta_{\text{reservoir}}=f$ (mixing, selection, isotope fractionation), is introduced here. The effect of mixing, selection and isotopic fractionation (especially steady or non-steady state) has been observed in the isotopic responses of each of the ILSSs.
- (4) A new tool for isotope-enabled model intercomparison has been introduced: the iPILPS plot. The iPILPS plot gives a quick summary of the annual isotope mass balance, just as the PILPS sensible

and latent heat plot has been used to summarize annual energy budgets (e.g. Chen et al., 1997). Although there are presently too few isotope-enabled land-surface schemes available to be able to properly investigate the relationships between isotope partitioning and model complexity, this plot has been shown here to reveal aspects of LSS characteristics not seen in gross water and energy analyses.

- (5) Finally, we have established that observational campaigns should measure both $\delta^{18}\text{O}$ and $\delta^2\text{H}$ in order to facilitate the comparison between observations and isotopically enabled models, with the aim of reducing the range of differences among current ILSSs.

Acknowledgments

We are very grateful to all the ILSS team members who assisted in the creation of the isotopic schemes and in these experiments. We are also grateful to three anonymous reviewers who made many substantive suggestions by means of which we have greatly improved this intercomparison.

References

- Aleinov, I., Schmidt, G., 2006. Water isotopes in the GISS model land surface scheme. *Global and Planetary Change* 51, 108–120. doi:10.1016/j.gloplacha.2005.12.010.
- Chen, T.H., Henderson-Sellers, A., Milly, P.C.D., Pitman, A.J., Beljaars, A.C.M., Polcher, J., Abramopoulos, F., Boone, A., Chang, S., Chen, F., Dai, Y., Desborough, C.E., Dickinson, R.E., Dumenil, L., Ek, M., Garratt, J.R., Gedney, N., Gusev, Y.M., Kim, J., Koster, R., Kowalczyk, E.A., Laval, K., Lean, J., Lettenmaier, D., Liang, X., Mahfouf, J.-F., Meinelkamp, H.-T., Mitchell, K., Nasonova, O.N., Noilhan, J., Robock, A., Rozensweig, C., Schaake, J., Schlosser, A., Schulz, J.P., Shao, Y., Shmakin, A.B., Verseghy, D.L., Wetzal, P., Wood, E.F., Xue, Y., Yang, Z.-L., Zeng, Q., 1997. Cabauw experimental results from the project for intercomparison of land-surface parameterization schemes. *Journal of Climate* 10, 1194–1215.
- Craig, H., Gordon, L.I., 1965. Deuterium and oxygen 18 variations in the ocean and marine atmosphere. In: Tongiorgi, E. (Ed.), *Stable Isotopes in Oceanographic Studies and Paleotemperatures*. Lab. Geologia Nucleare, Pisa, Italy, pp. 9–130.
- Cole, J.E., Rind, D., Webb, R., Jouzel, J., Healy, R., 1999. Global controls on interannual variability of precipitation $\delta^{18}\text{O}$: the relative roles of temperature, precipitation amount, and vapor source region. *Journal of Geophysical Research* 104, 14223–14235.
- Desborough, C.E., 1999. Surface energy balance complexity in GCM land surface models. *Climate Dynamics* 15, 389–403.
- Dickinson, R.E., Henderson-Sellers, A., Kennedy, P.J., Wilson, M.F., 1986. Biosphere–Atmosphere Transfer Scheme (BATS) for the NCAR Community Climate Model, NCAR Technical Note TN-275.
- Fischer, M.J., 2006. ICHASM, a flexible land-surface model that incorporates stable water isotopes. *Global and Planetary Change* 51, 121–130. doi:10.1016/j.gloplacha.2005.12.008.
- Fischer, M., Sturm, K., 2006. This issue. REMOiso forcing for the IPILPS Phase 1 experiments and the performance of REMOiso in three domains. *Global and Planetary Change* 51, 73–89. doi:10.1016/j.gloplacha.2005.12.006.
- Gat, J.R., 1996. Oxygen and hydrogen isotopes in the hydrologic cycle. *Annual Review of Earth and Planetary Sciences* 24, 225–262.
- Gonfiantini, R., 1986. Environmental isotopes in lake studies. In: Fritz, P., Fontes, J.Ch. (Eds.), *Handbook of Environmental Isotope Geochemistry*. Elsevier, N.Y., pp. 113–168.
- Henderson-Sellers, A., 2006. Improving land-surface parameterization schemes using stable water isotopes: introducing the iPILPS initiative. *Global and Planetary Change* 51, 3–24. doi:10.1016/j.gloplacha.2005.12.009.
- Henderson-Sellers, A., Irannejad, P., McGuffie, K., Pitman, A.J., 2003a. Predicting land-surface climates—better skill or moving targets? *Geophysical Research Letters* 30 (14), 1777–1780.
- Henderson-Sellers, A., Irannejad, P., McGuffie, K., Sharmeen, S., Phillips, T.J., McGuffie, K., Zhang, H., 2003b. Evaluating GEWEX CSES’ simulated land-surface water budget components. *GEWEX News* 3–6 (August).
- Jouzel, J., Koster, R.D., Joussame, S., 1996. Climate reconstruction from water isotopes: what do we learn from isotopic models? In: Jones, P.D., Bradley, R.S., Jouzel, J. (Eds.), *Climate Variations and Forcing Mechanisms of the Last 2000 Years*. Springer-Verlag, Berlin, pp. 213–242.
- Kistler, R., Kalnay, E., Collins, W., Saha, S., White, G., Woollen, J., Chelliah, M., Ebisuzaki, W., Kanamitsu, M., Kousky, V., van den Dool, H., Jenne, R., Fiorino, M., 2001. The NCEP-NCAR 50-year reanalysis: monthly means CD-ROM and documentation. *Bull. Am. Meteorol. Soc.* 82, 247–268.
- Koster, R.D., Milly, P.C.D., 1997. The interplay between transpiration and runoff formulations in land surface schemes used with atmospheric models. *Journal of Climate* 10, 1578–1591.
- Lai, C.T., Ehleringer, J., Bond, B., Paw U, K.T., 2006. Contributions of evaporation, isotopic non-steady state transpiration, and atmospheric mixing on the $\delta^{18}\text{O}$ of water vapor in Pacific Northwest coniferous forests. *Plant, Cell and Environment* 29 (1), 77–94.
- Manabe, S., 1969. Climate and ocean circulation: 1. The atmospheric circulation and the hydrology of the Earth’s surface. *Monthly Weather Review* 97, 739–805.
- Mathieu, R., Bariac, T., 1996. A numerical model for the simulation of stable isotope profiles in drying soils. *Journal of Geophysical Research* 101, 12685–12696.
- Pitman, A.J., 2003. The evolution of, and revolution in, land surface schemes designed for climate models. *International Journal of Climatology* 23, 479–510.
- Pitman, A.J., Henderson-Sellers, A., Desborough, C.E., Yang, Z.-L., Abramopoulos, F., Boone, A., Desborough, C.E., Dickinson, R.E., Gedney, N., Koster, R., Kowalczyk, E., Lettenmaier, D., Liang, X., Mahfouf, J.-F., Noilhan, J., Polcher, J., Qu, W., Robock, A., Rosenzweig, C., Schlosser, C., Shmakin, A.B., Smith, J., Suarez, M., Verseghy, D., Wetzal, P., Wood, E., Xue, Y., 1999. Key results and implications from Phase 1(c) of the project for intercomparison of land-surface parameterization schemes. *Climate Dynamics* 15, 673–684.
- Riley, W.J., Still, C.J., Torn, M.S., Berry, J.A., 2002. A mechanistic model of H_2^{18}O and C^{18}O fluxes between

- ecosystems and the atmosphere: model description and sensitivity analyses. *Global Biogeochemical Cycles* 16. doi:10.1029/2002GB001878.
- Rozenzweig, C., Abramopolous, F., 1997. Land-surface model development for the GISS GCM. *Journal of Climate* 10, 2040–2054.
- Sellers, P.J., Mintz, Y., Sud, Y.C., Dalcher, A., 1986. A simple biosphere model (SiB) for use within general circulation models. *Journal of the Atmospheric Sciences* 43, 505–531.
- Sturm, K., Hoffman, G., Langmann, B., Stichler, W., 2005. Simulation of $\delta^{18}\text{O}$ in precipitation by the regional circulation model REMOiso. *Hydrological Processes* 19, 3425–3444.
- Sturm, K., Hoffmann, G., Langmann, B., submitted for publication. Simulation of the stable water isotopes in precipitation over South America: comparing global to regional circulation models, *Journal of Climate*.
- Takata, K., Emori, S., Watanabe, T., 2003. Development of the minimal advanced treatments of surface interaction and runoff. *Global and Planetary Change* 38, 209–222.
- Twining, J., Stone, D., Tadros, C., Henderson-Sellers, A., Williams, A., 2006. Moisture isotopes in the biosphere and atmosphere (MIBA) in Australia: the Tumbarumba field campaign. *Global and Planetary Change* 51, 59–72. doi:10.1016/j.gloplacha.2005.12.005.
- Weiler, M., McGlynn, B.L., McGuire, K.J., McDonnell, J.J., 2003. How does rainfall become run-off? A combined tracer and runoff transfer function approach. *Water Resources Research* 39, 1315. doi:10.1029/2003WR002331.
- Yoshimura, K., 2006. Iso-Matsiro, a land surface model that incorporates stable water isotopes. *Global and Planetary Change* 51, 90–107. doi:10.1016/j.gloplacha.2005.12.007.